Department of Meteorology

THE UNIVERSITY OF OKLAHOMA

NORMAN, OKLAHOMA

DISCLAIMER NOTICE

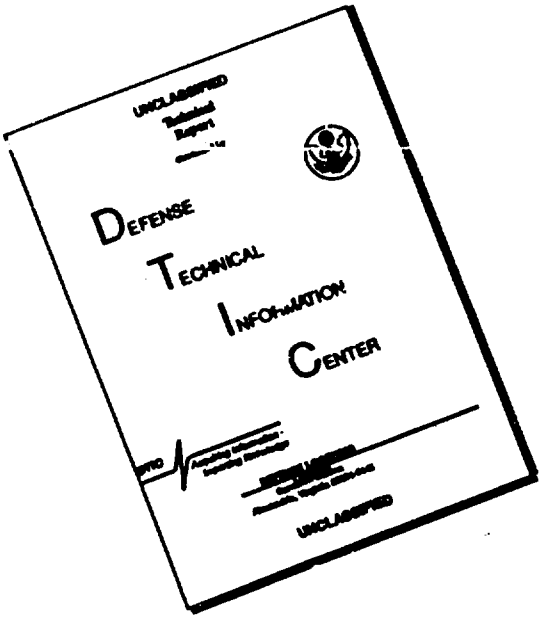

THIS DOCUMENT IS BEST QUALITY AVAILABLE. THE COPY FURNISHED TO DTIC CONTAINED A SIGNIFICANT NUMBER OF PAGES WHICH DO NOT REPRODUCE LEGIBLY.

OURI-1828-72-2

THE RELATIONSHIP BETWEEN HORIZONTAL MOISTURE CONVERGENCE AND SEVERE STORM OCCURRENCES

by

WILLIAM R. NEWMAN

NOAA Grant #N22-47-72(G) January 1972

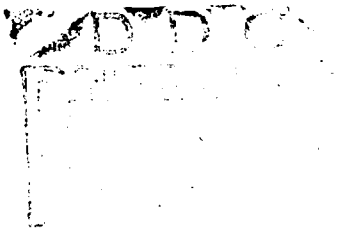

ABSTRACT

An objective analysis of the wind and mixing ratio using three-hourly surface observations was used to obtain patterns of horizontal moisture convergence over the eastern two-thirds of the United States. Sixty-three segments of time periods during April and May 1970, were examined. All cases chosen had severe weather occurring during some portion of the entire period.

A comparison was made between the fields of horizontal moisture convergence and reported severe weather occurrences. It was found that severe weather tends to develop at or closely after the time of strongest moisture convergence. Results of a quantitative study indicate that it may be beneficial to calculate horizontal moisture convergence on an hourly basis for use as a severe weather predictor.

LIST OF SYMBOLS

a	mean radius of the earth
b	one half the length of the minor axis of the ellipse used in the weight factor
D	distance from the grid point to the boundary of the elliptic region along the direction of the position vector locating the station with respect to the grid point
d	distance between the grid point and observation point
e	vapor pressure
MC	horizontal moisture convergence
p	pressure
q	mixing ratio
t_d	dew-point temperature (Celsius)
U	zonal component (along the X-axis) of $\mathbf{V}$
u	component of $\hat{\mathbf{V}}$ along the x-axis
$\mathbf{V}$	horizontal wind velocity
V	meridional component (along the Y-axis) of $\mathbf{V}$
v	component of $\hat{\mathbf{V}}$ along the y-axis
W	weight factor used in objective analysis
X	curvilinear distance along a latitude circle
x	axis of a rectangular grid along a standard longitude on the image plane of a polar stereographic map projection
Y	curvilinear distance along a longitude circle
y	axis of a rectangular grid perpendicular to a standard longitude on the image plane of a polar stereographic map projection

α	ratio of the length of major to minor axis in the elliptic weight factor
β	cosine of the angle between the vectors of wind velocity at a grid point and at an observation point
φ	latitude
φ_o	standard latitude (60N)
σ	image scale factor

1. INTRODUCTION

Areas of possible severe weather development are normally delineated with the aid of many parameters and indices (U.S. Weather Bureau, 1956; Miller, 1967). Parameters considered to be important include low-level moisture, vertical motion (or convergence), and stability. An index combining moisture with a kinematic quantity, such as divergence, has been shown by many investigators to relate well to areas of convective activity and severe weather occurrence (e.g., Sasaki et al., 1967).

In an early model developed by Beebe and Bates (1955) the concept of "divergence over convergence" is used to describe how low-level convergence produces parcel instability and causes moisture to be carried upward. Recent work by Stuart and Krishnamurti (1970) lends further support to the importance of the above concept. In a study of mesoscale convergence related to cumulus activity over the coastal area of the Japan Sea, Matsumoto et al. (1967) concluded that active cumulus convection whose tops exceeded 5000 m exists only in the mesoscale convergence zone of the order of 10^{-4} sec^{-1} and that areas of convergence moved coincidentally with the convective activity. A good correlation was also found by Hudson (1971) between convective activity and fields of horizontal moisture convergence over the United States computed for a layer extending from the surface to 10,000 ft.

Earlier work by Breiland (1958), concerning the development of instability lines, stressed the importance of horizontal convergence

in the lower levels in a region of favorable moisture and temperature distributions. The importance of using quantities that depend on the field of motion to identify areas of severe storm formation is also discussed by Endlich and Mancuso (1968). Specifically, the product of vertical motion and available moisture was found to relate well to areas where severe storms develop.

Until very recently (e.g., Lewis, 1971) all of the computations mentioned thus far have been calculated either over a small area on a meso-scale using surface and/or upper air data, or on a synoptic-scale using upper air data alone. The fact that a correlation was found between moisture convergence and convective activity using rawinsonde data, where the average distance between stations is approximately 200 n mi, strengthens the feasibility of trying to relate calculations on a synoptic-scale to mesoscale weather phenomena using surface data. Work by Lewis (1971) demonstrates that this is practical and possible with the use of proper objective analysis routines presently available.

A very simplified approach to the role of horizontal moisture convergence in the development of thunderstorm activity has been taken in this paper. Objectively analyzed fields of surface mixing ratio and surface wind components are combined to calculate fields of horizontal moisture convergence. Three-hourly surface observations are used as the source of data. For simplicity the effects of surface friction and topography are ignored. The moisture convergence computed from the surface data is assumed to represent the moisture convergence on

a horizontal plane near the ground. In this paper, the term horizontal moisture convergence is synonymous with moisture convergence at the surface of the earth. The convention has been taken that positive values of moisture convergence indicate moist air advection and velocity convergence.

2. DISCUSSION OF DATA AND METHOD OF ANALYSIS

Five cases were studied covering the periods of 62 time segments (see Table 1). These periods range in length from 18 hrs to two and a half days (6 to 20 three-hourly observation times). All cases chosen were days where severe storms had occurred, but, included several different types of synoptic situations. Observations utilized in the computations of mixing ratio and horizontal moisture convergence are stored on the National Severe Storm Forecast Center (NSSFC) Surface Data Tape. The data used for each station was latitude, longitude, temperature (deg C), dew point (deg C), wind direction and speed (knots), and station pressure (mb).

Mixing ratios were computed for each surface station using Tetens' empirical formula for vapor pressure

$$e = 6.108 \exp\left(\frac{a\ t_d}{b + t_d}\right),$$

where $a = 17.269388$, $b = 237.3$, and t_d is the surface dew point in degrees Celcius, together with the definition of mixing ratio

$$q = \frac{.622\ e}{p - e},$$

where q is the mixing ratio (gm kg^{-1}), p is the surface station pressure in millibars, and e is the vapor pressure (mb).

TABLE 1. SURFACE DATA

First observation time in cases	Number of consecutive observation times in case
0600 GMT 12 April 1970	8
1200 GMT 15 April 1970	6
0000 GMT 18 April 1970	18
0600 GMT 20 April 1970	20
0000 GMT 11 May 1970	10

Before an objective analysis procedure is employed some consideration must be given to the type of data being analyzed and the desired results sought from the analysis scheme. The correlation sought here is one between synoptic-scale patterns and mesoscale weather phenomena. If such a correlation is to be found it seems desirable that the final analyzed fields be free of small-scale irregularities, such as those causes by local terrain or individual thunderstorms in the vicinity of the observation point, yet be able to portray necessary detailed flow features and retain spatial gradients as indicated by observations. According to Endlich and Mancuso (1968) it is also desirable to avoid assumptions of quasi-geostrophic balance and adiabatic motion which do not apply to squall lines and thunderstorms. With these goals in mind the following objective analysis procedure was developed.

2.1 Objective Analysis Scheme

The area of analysis includes most of the continental United States between the Rocky Mountains and the Atlantic Ocean. This area is covered by a 21 x 27 grid network (see Fig. 1) with a grid interval of approximately 68.5 n mi. The average number of surface stations inside the grid network was 268, and the average distance between surface stations is approximately one gridlength.

The scheme of the objective analysis is a successive approximation procedure similar to that developed by Cressman (1959). However, the procedure used here includes a modification which allows observations within an elliptical region to correct previously determined estimates of the analysis at grid points and results in a desirable selective smoothing of the fields along the direction of the flow (Inman, 1970). The weight, W, applied to any observation within this region is determined by

$$W = \beta^2 \frac{D^2 - d^2}{D^2 + d^2} ,$$

where d is the distance between the grid point and the observation point, D is the distance from the grid point to the boundary of the elliptical region along the direction of the position vector locating the station with respect to the grid point, and β is the cosine of the angle between the wind velocity vector at the grid point, and the wind velocity vector at the observation point. W is set to zero if β is less than zero. D^2 is calculated according to

$$D^2 = \frac{b^2}{1 - (\frac{\alpha^2 - 1}{\alpha^2}) \cos^2\theta} \quad ,$$

where b is one half the length of the minor axis of the elliptical region, α is the ratio of the length of the major axis to that of the minor axis, and θ is the angle between the position vector locating the observation and the wind velocity vector at the grid point.

The analysis of the wind fields utilized later in the analysis of the mixing ratio fields, were determined using the values of b and α given in Table 2 on three successive scans through the data. Values of b and α used in analyzing the fields of mixing ratio are shown in Table 3.

As stated above the analyzed values of the wind at each grid point were used for the analysis of the fields of mixing ratio. In other words, instead of using the reported wind data at an observation point to determine β and θ in the correction factor to be applied at each grid point, interpolated values for each observation point calculated from the analyzed wind field for that time segment were utilized.

TABLE 2

VALUES OF b AND α USED FOR THE WIND ANALYSIS

FOR THREE SCANS THROUGH THE DATA

1st Scan

Pass	b (grid increment)	α
1	4	1 (circular)
2	2½	2
3	2	2

2nd Scan

Pass	b (grid increment)	α
1	3	2
2	2½	2
3	2	2

3rd Scan

Pass	b (grid increment)	α
1	3	2
2	2½	2
3	2	2
4	1½	2

TABLE 3

VALUES OF b AND α USED FOR THE ANALYSIS

OF THE FIELDS OF MIXING RATIO

Pass	b (grid increment)	α
1	4	1 (circular)
2	$2\frac{1}{2}$	2
3	$1\frac{1}{2}$	2

3. COMPUTATION OF HORIZONTAL MOISTURE CONVERGENCE

Analyzed values of mixing ratio and wind (u- and v-components) were used to calculate the horizontal moisture convergence patterns. In spherical polar coordinates the two dimensional horizontal moisture convergence (MC) is:

$$MC = - \nabla_H \cdot (q\vec{V}) = - \left[\frac{\partial (qU)}{\partial X} + \frac{\partial (qV)}{\partial Y} - \frac{qV\tan\varphi}{a}\right] , \qquad (1)$$

where $\vec{V}$ is the horizontal wind velocity, q is the mixing ratio (gm kg^{-1}), U and V are zonal and meridional components of V, respectively, X and Y are curvilinear distances along latitude and longitude circles, respectively, a is the mean radius of the earth, and φ is the latitude.

Using Phillips' (1957) expression for divergence on the polar stereographic map projection, (1) becomes

$$MC = - \sigma^2 \left[\frac{\partial (qu/\sigma)}{\partial x} + \frac{\partial (qv/\sigma)}{\partial y}\right] . \qquad (2)$$

In (2) σ is the image scale factor,

$$\sigma = \frac{1 + \sin\varphi_o}{1 + \sin\varphi} ,$$

φ_o is the standard latitude 60N, and u and v are the components of the horizontal wind along the x- and y-axis, respectively (positive x-axis south; positive y-axis east), of a rectangular grid on the image plane.

For our purposes the image surface is a plane which passes through the earth at the standard latitude.

As defined in (2) the horizontal moisture convergence (MC) may be expanded to show two parameters frequently used to relate the kinematics of the atmosphere to thunderstorm formation: velocity divergence and the advection of moisture.

$$MC = -\sigma^2\{q[\frac{\partial(u/\sigma)}{\partial x} + \frac{\partial(v/\sigma)}{\partial y}] + (\frac{u}{\sigma})\frac{\partial q}{\partial x} + (\frac{v}{\sigma})\frac{\partial q}{\partial y}\} . \qquad (3)$$

The first two quantities on the right-hand side of (3) are the product of the mixing ratio and velocity divergence, and will be referred to simply as the divergence term. The last two quantities make up the advection term.

These terms tend to have largest negative values under conditions of horizontal convergence (first term negative) and advection of moist air (second term negative). Thus, MC is a measure of an inflow of moist air and upward motion near the surface.

The effect of orography is considered to be relatively insignificant in comparison to the terms appearing in (3) and is neglected in this study. Therefore, (3) will be used to approximate the horizontal moisture convergence at the surface of the earth. A discussion of the orographic effect is presented in Appendix A.

The values of MC were calculated at the interior grid points using the following finite difference equation, corresponding to (3):

$$MC_{i,j} = -\frac{\sigma^2_{i,j}}{2\Delta}\{q_{i,j}[(\frac{u}{\sigma})_{i+1,j} - (\frac{u}{\sigma})_{i-1,j} + (\frac{v}{\sigma})_{i,j+1} - (\frac{v}{\sigma})_{i,j-1}] + (\frac{u}{\sigma})_{i,j}(q_{i+1,j} - q_{i-1,j}) + (\frac{v}{\sigma})_{i,j}(q_{i,j+1} - q_{i,j-1})\}, \quad (4)$$

where Δ is the distance between grid points (Δ = 127 km).

3.1 Comparison of Terms

The surface synoptic pattern and radar summary for 0000 GMT 19 April 1970 (Figs. 2 and 3, respectively) and the accompanying fields of advection of moisture (Fig. 4), divergence (Fig. 5), and horizontal moisture convergence (Fig. 6) will be used to illustrate the relative magnitudes of the terms appearing in Eq. (3).

The surface chart for this time showed a low pressure center over central Kansas with an occluded front extending out of the low pressure area over eastern Kansas becoming a cold front across central Oklahoma and central Texas. A warm front stretched from southeastern Kansas to eastern Tennessee. As shown by radar a broken line of thunderstorms and heavy rainshowers extended from southeastern Kansas, through eastern Oklahoma, into central Texas. Widespread rainshowers and thunderstorms were occurring in a large portion of the area from

the Gulf Coast of Texas to the southern Great Lakes region. Areas of thunderstorms were also located over central Texas, the Texas panhandle, and western Kansas.

The moisture advection pattern for this time is typified by moderate moist air advection ahead of the surface frontal system in the Mid-West with strong dry air advection over northwestern Oklahoma and south-central Kansas behind the frontal system. The area of dry air advection behind the cold front corresponds well to the echo-free region over western Oklahoma and central Kansas.

Areas of divergence at this time are related very well to areas of diffluence over the Great Lakes region, the Carolinas, and western Texas (Fig. 5). A tongue of moderate convergence extending from the Gulf Coast of Texas to central Oklahoma occurs along the surface cold front, with a maximum centered over central Kansas coincident with the surface low pressure center.

Although the overall horizontal moisture convergence pattern is seen to be similar to the divergence pattern there are significant differences between the two. For instance, the tongue of velocity convergence over eastern Texas as revealed by Fig. 5 is located further to the west and magnified slightly in the MC pattern (Fig. 6) as a result of stronger moist air advection in this region. Comparison of this area with the corresponding radar summary (Fig. 3) indicates that the resulting pattern of MC yields a much better correlation with the heavy convective activity occurring over the central Texas region than does the pattern of velocity divergence. This aspect was not unique to

this case and it was deemed advantageous to utilize the field of MC rather than just the divergence pattern to delineate areas of possible severe weather development.

An estimate of the magnitudes of the horizontal moisture convergence (MC), advection term, and divergence term was obtained by calculating the mean of their absolute values over the entire grid network for 0000 GMT 19 April 1970. A crude attempt was made to separate large-scale features from small-scale features by isolating the area around the low pressure center over Kansas and the front extending over Oklahoma and Texas, and labeling this small-scale (sub-synoptic). The remaining grid points in the network were categorized as synoptic-scale. These results as well as the ratios of the mean absolute values of advection and divergence to horizontal moisture convergence for the period 0000 GMT 19 April 1970 are summarized in Tables 4 and 5.

TABLE 4. MEAN ABSOLUTE VALUES OF ADVECTION, DIVERGENCE, AND HORIZONTAL MOISTURE CONVERGENCE TERMS FOR 0000 GMT 19 APRIL 1970 (VALUES ARE x 10 gm kg^{-1} hr^{-1})

Term	Large-scale (386 grid points)	Small-scale (70 grid points)	Whole grid 456 grid points)
$\overline{\nabla_H \cdot (q\vec{V})}$	2.701	8.686	3.62
$\overline{\vec{V} \cdot \nabla_H q}$	0.916	2.049	1.089
$\overline{q \nabla_H \cdot \vec{V}}$	2.468	9.044	3.477

TABLE 5. RATIOS OF THE MEAN ABSOLUTE ADVECTION AND DIVERGENCE TERMS TO THE MEAN ABSOLUTE HORIZONTAL MOISTURE CONVERGENCE FOR 0000 GMT 19 APRIL 1970

Ratio of Terms	Large-scale (386 grid points)	Small-scale (70 grid points	Whole grid (456 grid points)
$\frac{\lvert\overline{\nabla\cdot\nabla_H q}\rvert}{\lvert\overline{\nabla_H\cdot(q\nabla)}\rvert}$	0.34	0.24	0.30
$\frac{\lvert\overline{q\nabla_H\cdot\nabla}\rvert}{\lvert\overline{\nabla_H\cdot(q\nabla)}\rvert}$	0.914	1.04	0.96

From Tables 4 and 5 it is seen that of the two terms of the right-hand side of Eq. (3) the divergence term predominates for both large-scale and small-scale features, and is almost an order of magnitude larger than the advection term in the case of small-scale features for this particular case.

3.2 Results of Analysis

Two cases will be discussed to illustrate the results of the objective analysis procedure and the relationship found between the fields of moisture convergence and severe weather occurrences. Quantitative results will be discussed in 4.

Case 1 -- 2100 GMT 19 April to 0000 GMT 20 April 1970

Surface charts, radar summaries, severe weather occurrences, and fields of horizontal moisture convergence for this period are given in Figs. 7 through 14. As seen from Figs. 7 and 11 low pressure dominated the area of analysis during the period. The pair of lows situated along the quasi-stationary front over southern Illinois and Iowa at 2100 GMT 10 April combine into one center of low pressure over northern Illinois by 0000 GMT 20 April. Another low pressure center drifted slowly southward over Colorado during this three hour period, however, no significant weather was associated with this feature. A trough of low pressure lagged behind the cold frontal system moving eastward through the Mississippi Valley while a quasi-stationary front remained over the Ohio Valley and mid-Atlantic states. A squall line moving through central and eastern Alabama triggered several tornadoes and strong winds in Mississippi, Tennessee, and Florida during the afternoon and evening hours.

Radar charts for the period (Figs. 8 and 12) indicated a line of heavy thunderstorms along the squall line over Alabama, and an area of broken thunderstorms along and east of the cold front. Several lines of moderate rain showers and thunderstorms remained behind the cold front, and ahead of the low pressure trough.

Severe weather reported during the three hour period after 2100 GMT 19 April (Fig. 9) occurred between the cold front and trough of low pressure along the Mississippi River from northern Mississippi to southern Illinois near a center of maximum MC and along the axis

of maximum MC. The strong wind reported at 2135 GMT 19 April over central Tennessee developed along the northern edge of the squall line in an area of apparent weak divergence of horizontal moisture. The pattern of MC in this area was changing throughout the day, however, and it is possible that by the time of occurrence this area could have been in the leading edge of positive MC which was moving eastward into Tennessee. At 0000 GMT 20 April a center of maximum MC (Fig. 14) was located over east-central Illinois with severe weather during the next three hour period being reported over southern Illinois and central Indiana (see Fig. 13). Tornadoes were also reported over the Florida panhandle and west-central Georgia corresponding to a maximum of MC in this region.

The 500-mb analysis for 0000 GMT 20 April 1970 indicated the presence of a strong jet (75-80 kt) split over both of these regions, and the movement of the center of MC from northwestern Arkansas to central Illinois is approximated by one half the 500-mb wind vector over this area. It is also noted from Figs. 10 and 14 that the area of reported severe weather is closely correlated with the intersection of the jet axis and the axis of maximum MC.

Case 2 -- 1800 GMT 29 April to 0300 GMT 30 April 1970

The synoptic situation for this case (see Figs. 15, 19, 23, and 27) is typified by a quasi-stationary front over southern New England extending westward over the Great Lakes region, and a cold frontal system over the Plains states which had been moving slowly

eastward prior to 1800 GMT 29 April. Severe weather outbreaks were widely scattered over the region from Texas to the Northern Plains states, and the Ohio Valley. Soundings taken at 1200 GMT the morning of the 29th indicated a large area of potentia ly unstable air south and east, respectively, of these two frontal system. A surface high pressure ridge located over the Gulf States provided a low-level southerly flow of moist air out of the Gulf over most of the Central United States.

At 1800 GMT 29 April several centers of MC were moving northward along the frontal system in the Mid-West. All severe weather which formed along this front occurred in regions of positive MC. Furthermore, radar summaries for this time period indicated that the heavier convective activity was coincident with areas of maximum positive MC.

The 500-mb flow (not shown) was characterized throughout the period by strong southwesterly winds over the Central United States. Unlike the previous case the axis of strongest winds (approximately 80 kt) was located 100 to 200 n mi to the west of the areas of maximum moisture convergence and severe weather outbreaks.

Of interest is the rapid development of convective activity over Indiana on the afternoon of the 29th of April. The radar summary at 1800 GMT (Fig. 16) showed this area to be echo-free. Within the next three hours an area of moderate to heavy thunderstorms had developed over central Indiana (Fig. 20). One report of hail (1 3/4 inches)

in this region occurred at 1924 GMT (Fig. 17) over Indianapolis. An outbreak of severe weather occurred between 2100 GMT and 0300 GMT (see Figs. 21 and 25). Interpolated values of MC over Indianapolis for 1200 GMT, 1500 GMT, and 1800 GMT were 0.01, -0.14, and 0.39 gm kg^{-1} hr^{-1}, respectively. Hence, shortly before the time of occurrence there was a definite increase in moisture convergence, and, although the value of 0.39 gm kg^{-1} hr^{-1} is not as high as might be expected, a closer look reveals that this area was characterized by potentially unstable conditions (morning soundings indicated a Lifted Index of -5 or less from central Indiana to eastern Kansas) and high moisture at the surface (mixing ratios in this area at 1800 GMT were in excess of 17 gm kg^{-1}).

From subjective examination of these cases it appears that an increase in horizontal moisture convergence occurs near the time of occurrence of a high percentage of severe weather events and that a relation with other synoptic features, such as location of upper level jets and areas of latent instability, exists and can be used to successfully delineate areas of severe weather development on an hourly or three-hourly basis. With these thoughts in mind a quantitative study was undertaken to determine more precisely the role of horizontal moisture convergence in severe storm development.

4. QUANTITATIVE STUDY

Because of the large number of severe weather occurrences reported during 18 to 20 April 1970 (153 reports of severe weather) this case was selected for an initial quantitative study. All reports of severe weather utilized in this paper were obtained from the National Severe Storms Forecast Center severe weather tape (WWVER). Reports of severe weather occurrences received at NSSFC are verified by regional meteorological personnel of the states involved before the information is entered on the WWVER tape. The information coded for each report includes type, state, day, month, year, time (CST), latitude, longitude, and remarks (i.e., hail size and wind speed, if applicable). The different types of weather and corresponding codes used at NSSFC are given in Table 6. It was convenient for this study, however, to categorize only the four types of weather shown in Table 7. The two different wind reports coded by NSSFC were integrated into one wind category for purposes of this study.

A method was sought to best exemplify the spatial and time distribution of the horizontal moisture convergence (MC) in relation to the reported severe weather occurrences. For this study surface data and, hence, patterns of MC were available only at three-hourly intervals. In general the times of the severe weather occurrences do not coincide with the surface data times. It is convenient, therefore, to define three-hourly time categories which will enable values

of MC to be calculated at regular intervals away from the time of occurrence. Seven time categories were chosen for this purpose and are shown in Table 8.

Values of MC at the points of occurrences were interpolated from the four surrounding analyzed grid point values for each of the seven different time categories. Plots of the average values of MC and the average normalized values of MC for each time category are shown in Figs. 31a and 31b, respectively. A graph of the individual values of MC versus the number of cases for category five is given in Fig. 32. As indicated in Fig. 31a, the maximum MC occurs in category five (0 to 3 hrs prior to time of occurrence), and increases significantly from category three (6 to 9 hrs prior to time of occurrence) for all types of severe weather occurrence. This is indicative, then, that a mechanism is available to lift moisture from the lower levels of the atmosphere somewhere in the time interval zero to six hours preceding the occurrence of severe weather.

The spatial distribution of MC was obtained by describing a 7x7 grid network centered on each point of severe weather occurrence for each time category. The grid interval is approximately 68.5 n mi and is identical to that used in the objective analysis routine. Therefore, values at each grid location surrounding the point of occurrence can easily be interpolated from the analyzed grid point values of MC.

The values of MC at each grid point were normalized by dividing all grid point values for each occurrence by the maximum value of MC

TABLE 6. NSSFC WWVER SEVERE WEATHER CODE

Report	Code
Tornado	4
Hail	5
Wind (65 kt or more - damaging winds)	6
Wind (50 to 64 kt - wind damage)	7
Extreme Turbulence	8
Funnel aloft (Pireps)	9
Funnel Cloud	10
Waterspout	11
Radar Report	57

TABLE 7. CATEGORIES OF SEVERE WEATHER

Category	Type of Weather
1	Tornado
2	Hail
3	Wind (equal to or greater than 50 kt)
4	Funnel Cloud

that occurred at the grid points surrounding the occurrence in any of the seven time categories. The normalized values were then averaged by summing over all occurrences and dividing by the number of values for each grid point. For the sake of brevity only categories three, four, five, and six will be illustrated here. In general categories one and two indicated weak horizontal moisture convergence at all grid points up to 15 hrs prior to the time of occurrence with higher values to the west of the point of occurrence and lower values to the east.

TABLE 8. CATEGORIES OF TIME INTERVALS

Category	Time Interval of Data
1	12 to 15 hrs prior to occurrence
2	9 to 12 hrs prior to occurrence
3	6 to 9 hrs prior to occurrence
4	3 to 6 hrs prior to occurrence
5	0 to 3 hrs prior to occurrence
6	0 to 3 hrs after occurrence
7	3 to 6 hrs after occurrence

Fig. 33 shows the normalized pattern six to nine hours prior to 126 severe weather occurrences. The point of occurrence is the center grid point and is indicated by a solid triangle. High values were located to the southwest of the center grid point and a relative

minimum was situated about two gridlengths southeast of the point of occurrence. By the time of the next category (see Fig. 34) values had increased significantly to the southwest of the center grid point with a north-south oriented axis of maximum MC situated approximately 1½ gridlengths to the west of the center grid point. The highest normalized values for the grid network, approximately 0.6, were observed in this category and were due to frontal influences or strong wind convergence zones ahead of a front, such as those associated with a dry line or squall line.

The axis of maximum MC moved towards the east during the next three hours and was located within one grid interval of the center point 0 to 3 hrs prior to 95 reported severe weather occurrences (see Fig. 35). A center of maximum MC was situated within two grid intervals to the southwest of the point of occurrence. Maximum normalized values had decreased slightly from the previous category, but, were still above 0.45. A strong gradient was noted to the west of the axis of maximum MC. This was a reflection of sinking motions associated with low-level divergence and rapid drying that normally occurs behind a cold frontal system such as the one in this case. The maximum value at the center grid point occurred during this time category and corresponds to the maximum indicated for category five as shown in Fig. 31b.

The next category (see Fig. 36) reflects that the axis of maximum MC had moved approximately one grid interval to the east of the point of occurrence. The normalized value at the center point had now fallen below 0.4. The eastward movement of the axis of MC continued

during the last category (not shown) with a continued decrease in the normalized value at the center grid point.

Results similar to those above were obtained from the analyzed fields of MC for two other cases for which a sufficient number of reports of severe weather were available. In each case, although maximum values and direction of movement varied, a maximum value of MC occurred at the severe storm location zero to three hours prior to the time of severe weather occurrence.

5. CONCLUSIONS

Estimates of the magnitude of the advection term and the divergence term from a limited case study indicate that the latter dominates the pattern of horizontal moisture convergence (MC). However, the combination of these two terms generally produces a better delineation of the areas of moderate to strong convective activity and severe storm development.

The patterns of MC can be used with other meteorological parameters to further delineate areas of possible severe storm development. A favored area of severe weather occurrence was found to be the intersection of the 500-mb jet with the axis of maximum MC.

The most important conclusion that may be stated from the results of the limited quantitative case study is that severe weather tends to develop at or closely after the time of greatest horizontal moisture convergence. Furthermore, the magnitude of the locally maximum horizontal moisture convergence increases rapidly during the several hours prior to the severe storm outbreak. Of further interest, it was noted that the average magnitude of MC near the time of occurrence for all types of severe weather studied was approximately 1 gm kg^{-1} hr^{-1}. It should be emphasized that this is only an average value and that a substantial amount of scatter occurred around this value. These results are very encouraging especially in view of the fact that such a large time interval was utilized. A closer examination of the time relationship between horizontal moisture convergence and occurrences

of severe weather is desirable. In particular it is felt that patterns of MC obtained from hourly (vice three-hourly) surface data may yield a more exact correlation with the areas of severe weather development.

ACKNOWLEDGMENTS

I wish to express my appreciation to Dr. Rex Inman for his suggestion of the area of investigation and for his invaluable guidance and encouragement throughout the writing of this thesis. My sincere thanks to Dr. Yoshikazu Sasaki for his critical review of the manuscript and his enthusiastic support of this work. I also wish to thank Frank P. Hall, Lt. Colonel, USAF (Ret.), for his helpful suggestions during the past year and Captains Pershing Hicks and Peter Soliz for their photographic assistance with the illustrations.

This research was done in connection with graduate study at the University of Oklahoma sponsored by the Air Force Institute of Technology and supported by the National Oceanic and Atmospheric Administration under research grant N22-47-72(G).

REFERENCES

Beebe, R. G., and F. C. Bates, 1955: A Mechanism for Assisting in the Release of Convective Instability, Mon. Wea. Rev., Vol. 83, pp. 1-10.

Breiland, J. G., 1958: Meteorological Conditions Associated with the Development of Instability Lines, J. Meteor., Vol. 15, pp. 297-302.

Cressman, G. P., 1959: An Operational Objective Analysis System, Mon. Wea. Rev., Vol. 87, pp. 367-374.

Endlich, R. M., and R. L. Mancuso, 1968: Objective Analysis of Environmental Conditions Associated with Severe Thunderstorms and Tornadoes, Mon. Wea. Rev., Vol. 96, No. 6, pp. 342-351.

Fankhauser, J. C., 1965: A Comparison of Kinematically Computed Precipitation with Observed Convective Rainfall, National Severe Storms Laboratory Report Number 25, September 1965, 28 pp.

Foster, D. S., 1964: Relationship Among Tornadoes, Vorticity Acceleration, and Air Mass Stability, Mon. Wea. Rev., Vol. 92, No. 7, pp. 339-343.

Hudson, H. R., 1971: On the Relationship Between Horizontal Moisture Convergence and Convective Cloud Formation, J. Meteor. Vol. 10, No. 4, pp. 755-762.

Inman, R. L., 1970: Papers on Operational Analysis Schemes at the National Severe Storms Forecast Center, NOAA Tech. Memo. ERLTM-NSSL 51, 91 pp.

Lewis, J. M., 1971: Variational Subsynoptic Analysis with Applications to Severe Local Storms, Mon. Wea. Rev., Vol. 99, No. 10, pp. 786-795.

Lewis, J. M., and T. H. Grayson, 1971: The Adjustment of Surface Wind and Pressure by Sasaki's Variational Matching Technique (submitted to J. of Appl. Meteor., October 1971).

Matsumoto, S., K. Ninomiya, and T. Akiyama, 1967: Cumulus Activities in Relation to the Mesoscale Convergence Field, J. Meteor. Soc. Japan, Vol. 45, No. 4, pp. 292-305.

Miller, R. C., 1967: Notes of Analysis and Severe Storm Forecasting Procedures of the Military Weather Warning Center, AWS Tech. Rept. No. 200, 125 pp.

Panofsky, H. A., 1968: Introduction to Dynamic Meteorology, The Pennsylvania State University, Pennsylvania, 243 pp.

Phillips, N. A., 1957: A Map Projection System Suitable for Large-Scale Numerical Weather Prediction, 75th Anniversary Volume of the Journal of Meteorology Society of Japan, pp. 262-267.

Sasaki, Y., 1970: Some Basic Formalisms in Numerical Variational Analysis, Mon. Wea. Rev., Vol. 98, No. 12, pp. 875-883.

Stuart, D. W., and T. N. Krishnamurti, 1970: Specifications of Meso-Scale Weather from Large-Scale Dynamical Calculations, Final Report No. 70-5, Florida State University, 79 pp.

U.S. Weather Bureau, 1956: Forecasting Tornadoes and Severe Thunderstorms, Forecasting Guide No. 1, Washington, D.C., 35 pp.

APPENDIX A: OROGRAPHIC EFFECTS

The equation for the horizontal moisture convergence in 3 is developed by assuming that the effect of orography can be neglected. In this section a comparison is made between the orographic term and the horizontal velocity divergence term in order to justify the above assumption.

The following symbols will be used to designate the variables:

- x,y: horizontal cartesian coordinates on the polar stereographic projection
- z : geometric height above the projection
- u : x-component of velocity
- v : y-component of velocity
- h : topographic height above mean sea level

An ordinate s is defined which will incorporate the orographic effect into the divergence term (see Fig. A-1).

$$s = z - h(x,y) \tag{A-1}$$

In the x,y,s,t system the horizontal velocity divergence is given by

$$\left.\frac{\partial u}{\partial x}\right)_z + \left.\frac{\partial v}{\partial y}\right)_z = \left[\left.\frac{\partial u}{\partial x}\right)_s + \left.\frac{\partial v}{\partial y}\right)_s\right] - \left[\frac{\partial u}{\partial s}\frac{\partial h}{\partial x} + \frac{\partial v}{\partial s}\frac{\partial h}{\partial y}\right] . \tag{A-2}$$

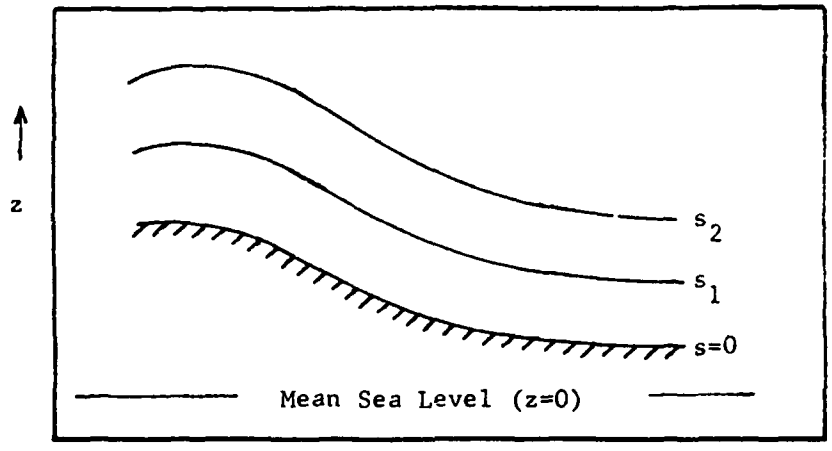

Fig. A-1. Orographic coordinate surfaces. (s=0 represents the surface of the earth.)

The terms on the right hand side of (A-2) are the horizontal velocity divergence on an s-surface and the orographic term, respectively. The magnitude of the first term can be estimated from the results found in Chapter III. From Table 4 the mean absolute value of the product of the mixing ratio and horizontal velocity divergence was found to be .3477 gm kg^{-1} hr^{-1}. If we assume a mixing ratio of the order of 10^{-2} (10 gm kg^{-1}) then it is readily seen that the corresponding velocity divergence is of the order of 10^{-5} sec^{-1}.

The magnitude of the second term in (A-2) can be estimated by assuming values of 10 m sec^{-1} per 5 km for the vertical wind shear, and 1 km per 1000 km for the slope of the terrain. This yields an order of magnitude of 10^{-6} sec^{-1} for the orographic term. Therefore, when the slope of the terrain is of the order of 10^{-3} or smaller the effect of orography will be negligible in comparison to the horizontal velocity divergence.

TABLE 9

LIST OF SYMBOLS FOR RADAR SUMMARY CHARTS

⊙	less than 0.1 coverage	amount of radar echo
◐	0.1 to 0.5 coverage	
◑	0.6 to 0.9 coverage	
⊕	over 0.9 coverage	
R	rain	Type of surface weather associated with echo
RW	rain showers	
S	snow	
SW	snow showers	
T	thunderstorm	
--	very light	intensity of precipitation
-	light	
no sign	moderate	
+	heavy	
++	very heavy	
U	unknown	
-+	decreasing rapidly	intensity tendency
--	decreasing slowly	
-	decreasing	
NC	no change	

+	increasing	intensity tendency
+-	increasing slowly	
++	increasing rapidly	
hhh	height of echo tops	height in hundreds of feet MSL
,hhh,	maximum height of echo tops	

LN preceding the weather type indicates a line of echoes; otherwise the symbols refer to an area of echoes.

The intensity tendency symbol follows intensity of the echo symbol and is preceded by a slash.

Example: LN TRW + / -- means that a line of thunderstorms and heavy rain showers are occurring and are decreasing slowly in intensity.

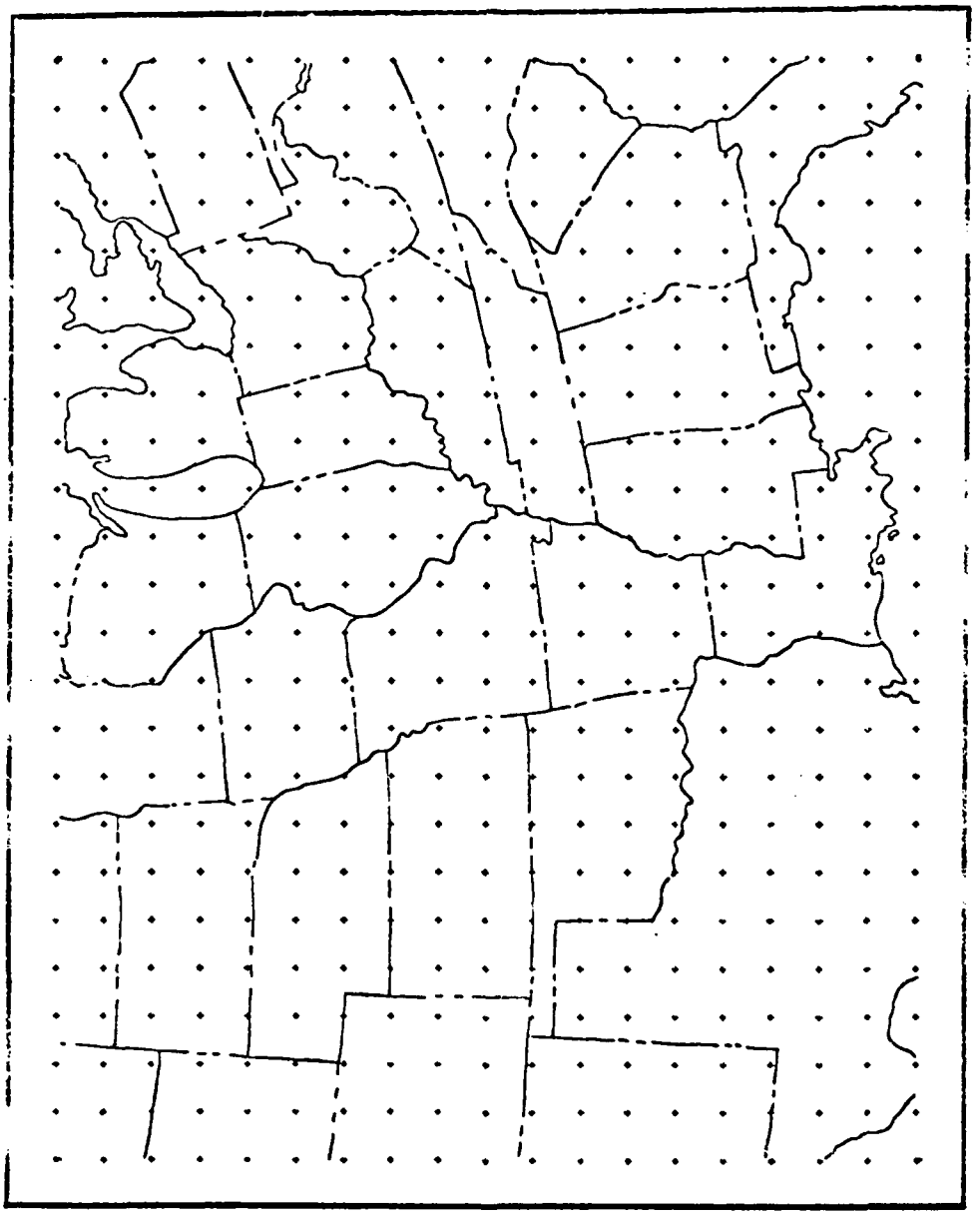

Fig. 1. Grid and area of analysis.

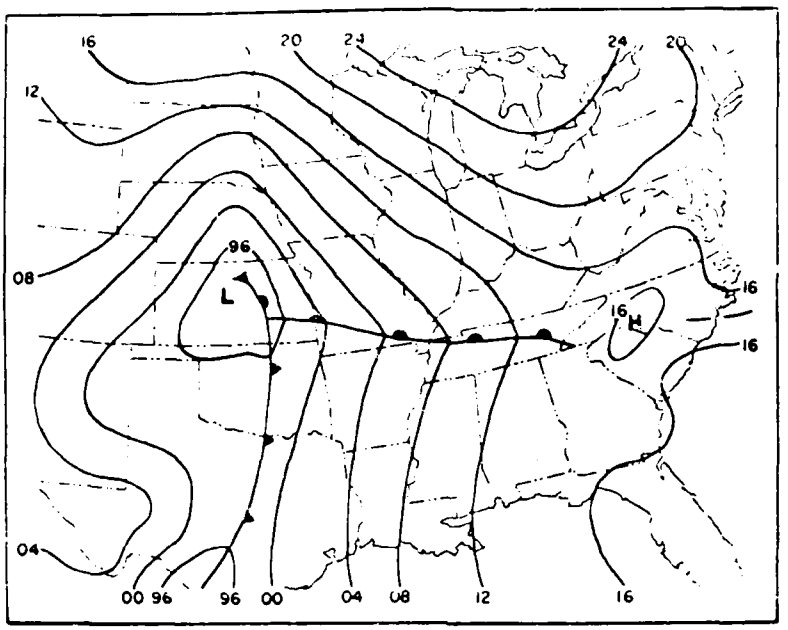

Fig. 2. Surface chart for 0000 GMT 19 April 1970.

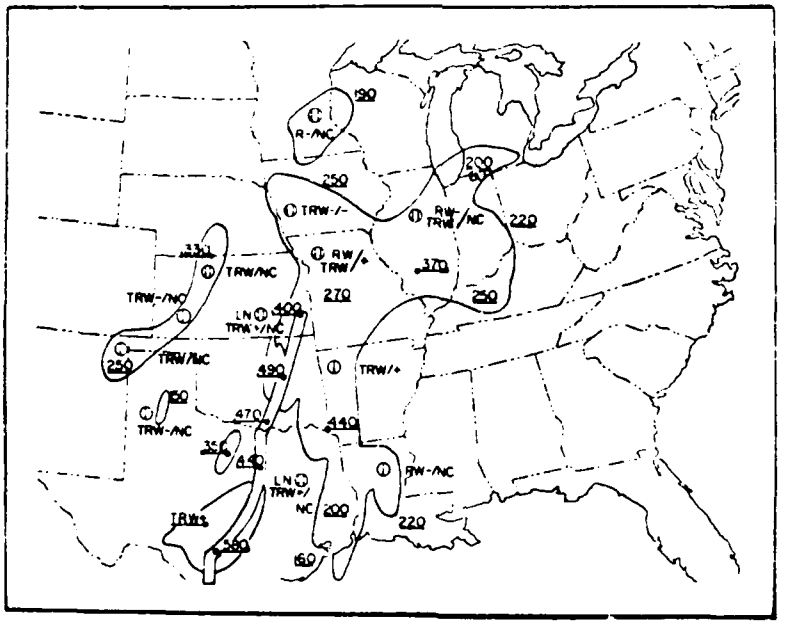

Fig. 3. Radar summary for 2345 GMT 18 April 1970.

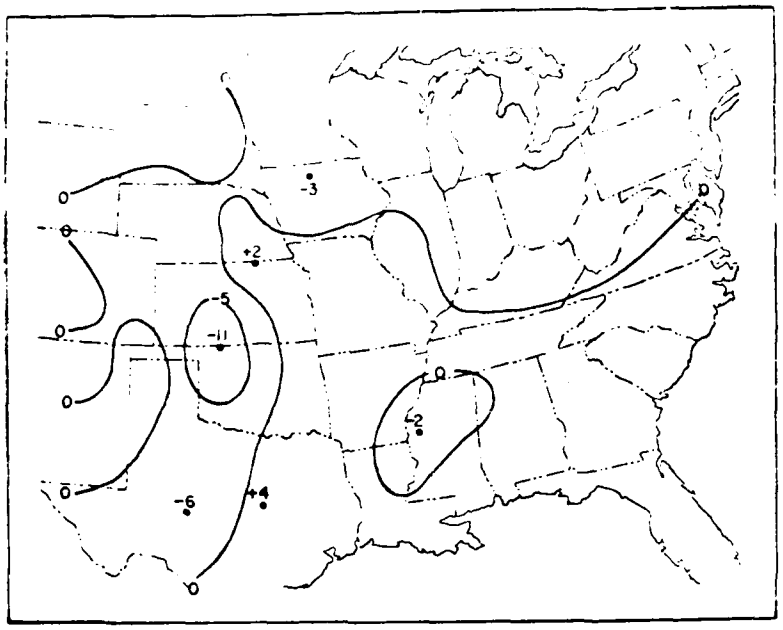

Fig. 4. Moisture advection for 0000 GMT 19 April 1970 (x 10 gm kg^{-1} hr^{-1}). Positive values indicate moist air advection.

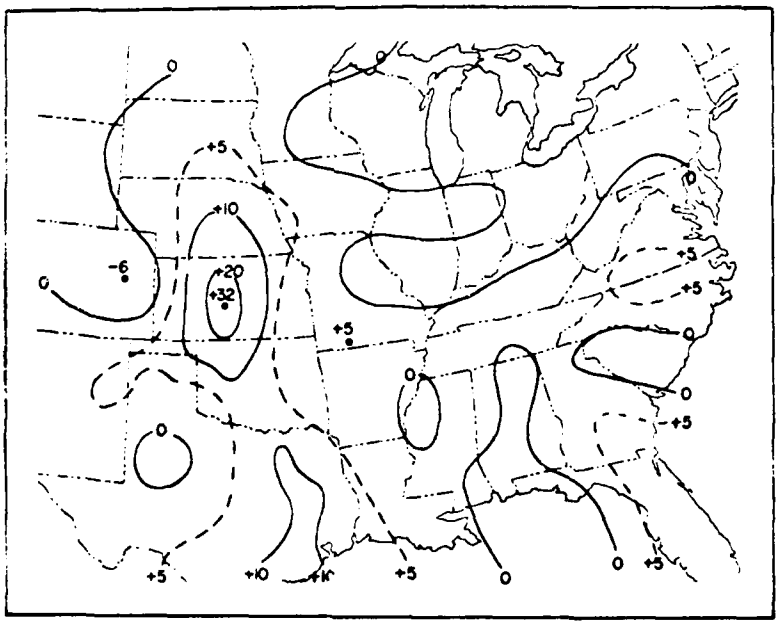

Fig. 5. Product of mixing ratio and velocity divergence for 0000 GMT 19 April 1970 (x 10 gm kg^{-1} hr^{-1}). Positive values indicate convergence.

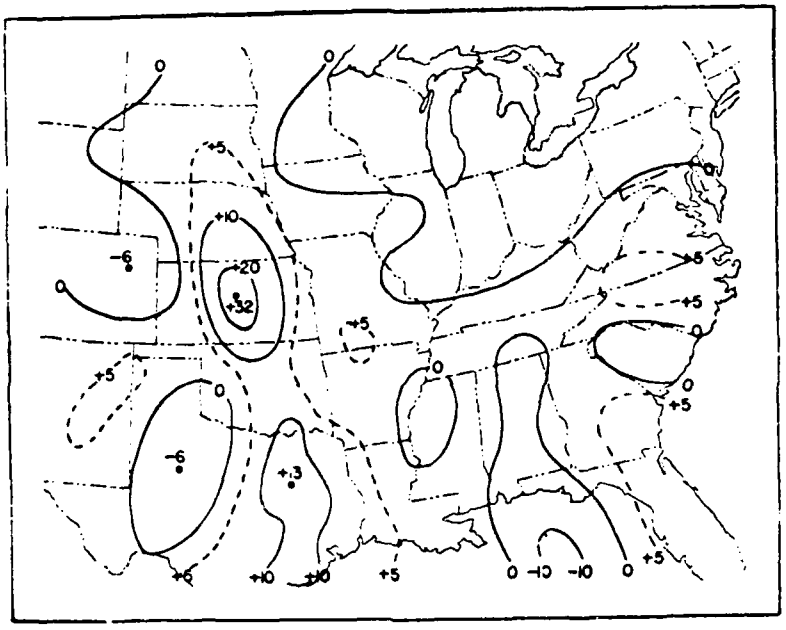

Fig. 6. Horizontal moisture convergence for 0000 GMT 19 April 1970 (x 10 gm kg^{-1} hr^{-1}). Positive values indicate convergence.

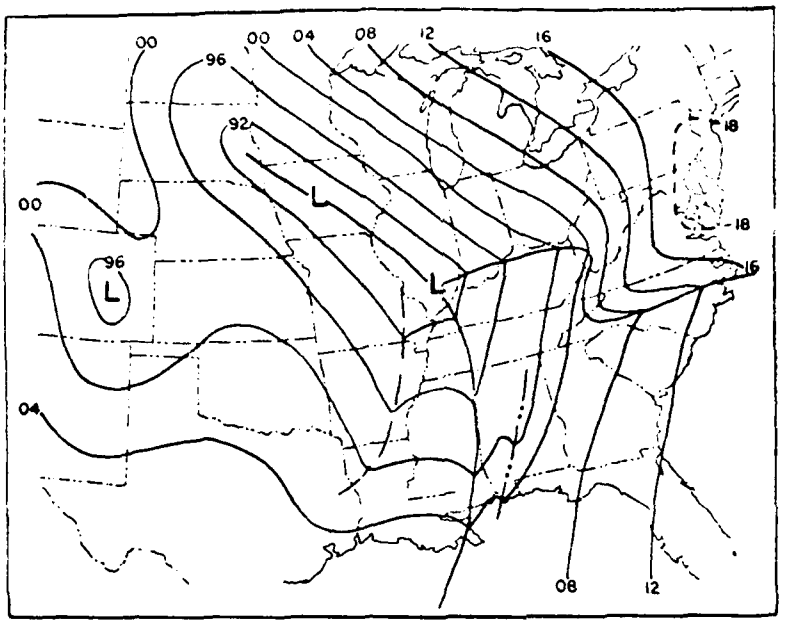

Fig. 7. Surface chart for 2100 GMT 19 April 1970.

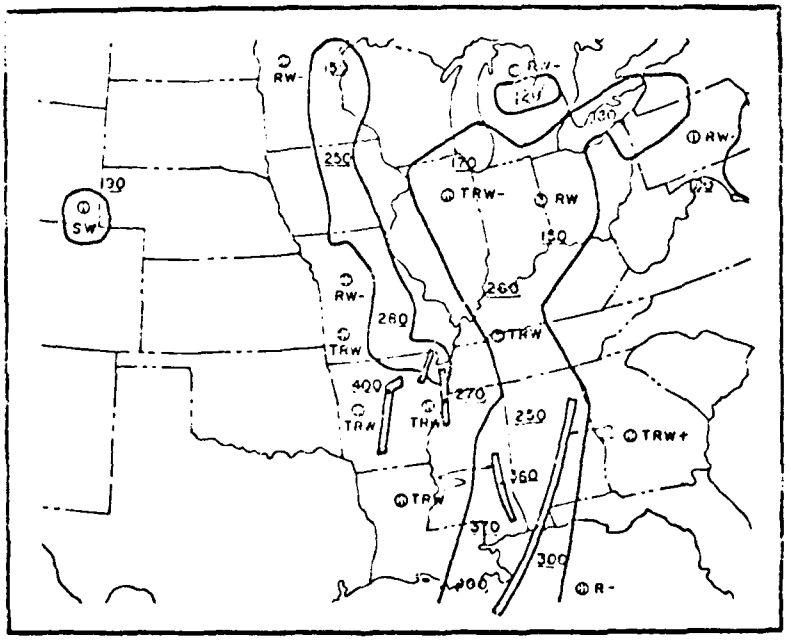

Fig. 8. Radar summary for 2045 GMT 19 April 1970.

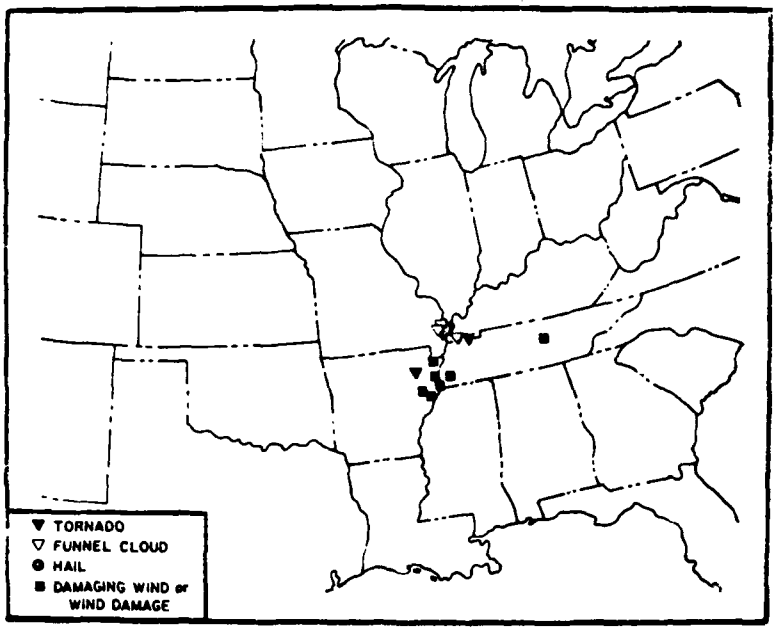

Fig. 9. Severe weather occurrences between 2100 GMT April and 0000 GMT 20 April 1970.

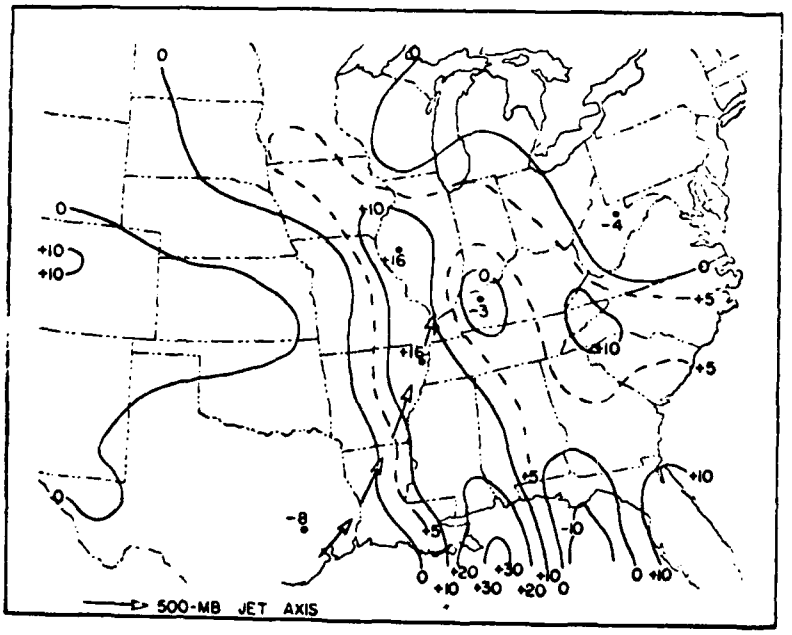

Fig. 10. Horizontal moisture convergence (x 10 g kg^{-1} hr^{-1}) for 2100 GMT 19 April 1970.

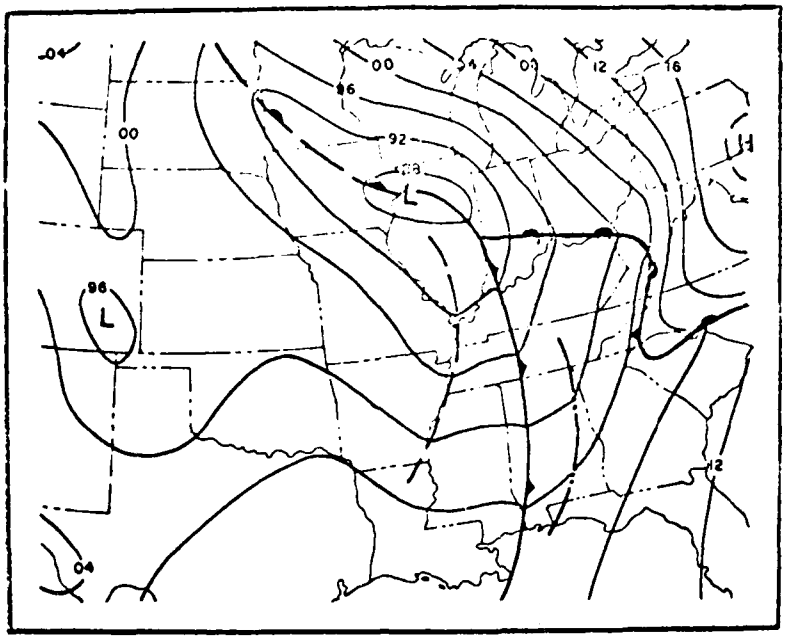

Fig. 11. Surface chart for 0000 GMT 20 April 1970.

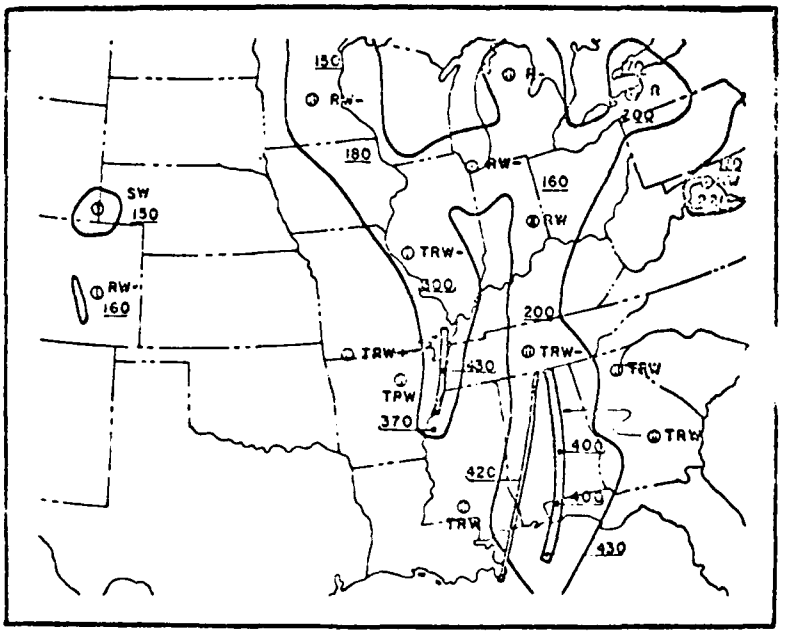

Fig. 12. Radar summary for 2345 GMT 19 April 1970.

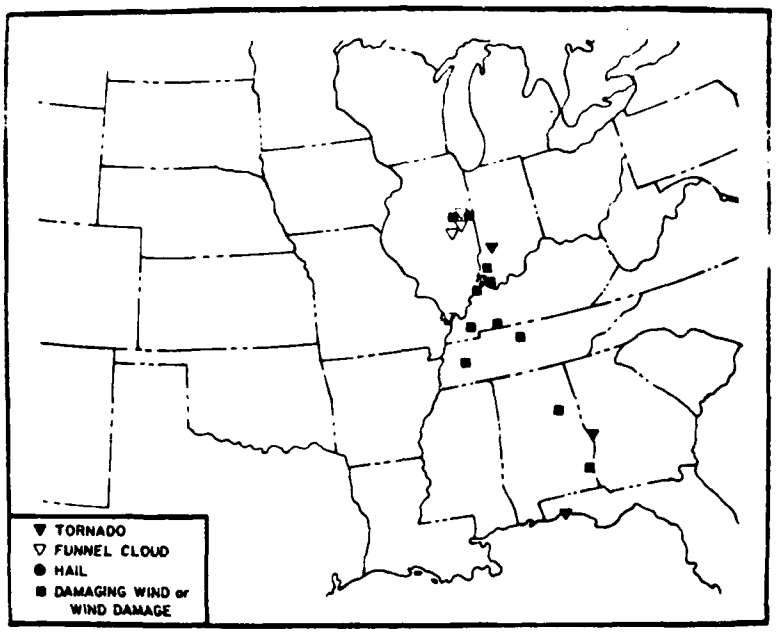

Fig. 13. Severe weather occurrences between 0000 GMT and 0500 GMT 20 April 1970.

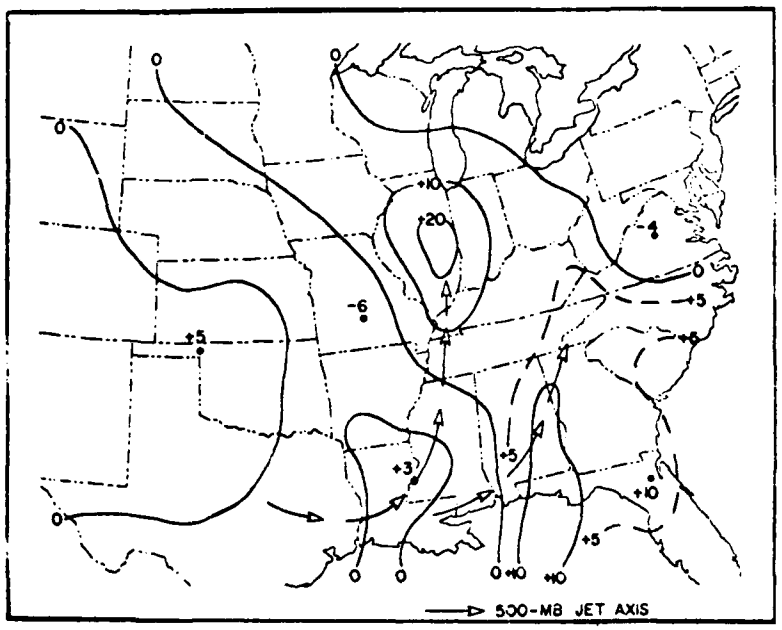

Fig. 14. Horizontal moisture convergence (x 10 gm kg^{-1} hr^{-1}) for 0000 GMT 20 April 1970.

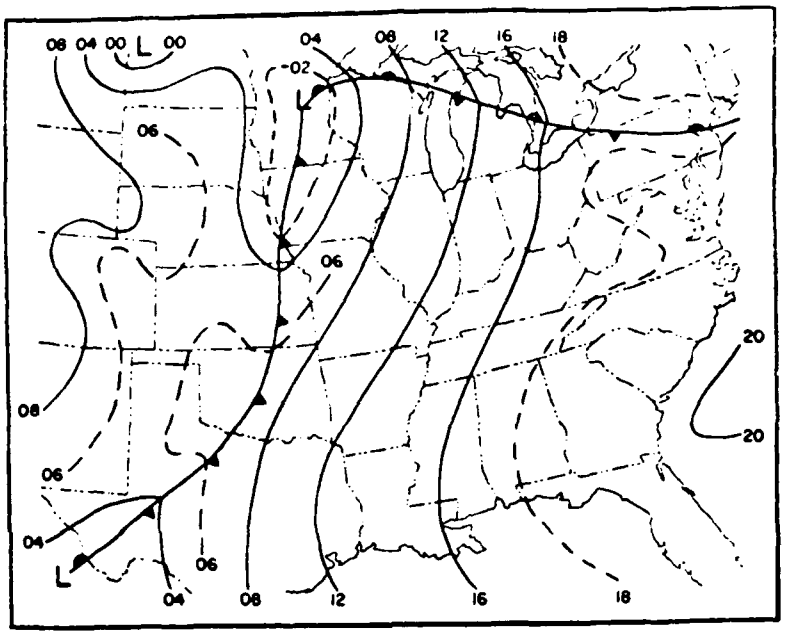

Fig. 15. Surface chart for 1800 GMT 29 April 1970.

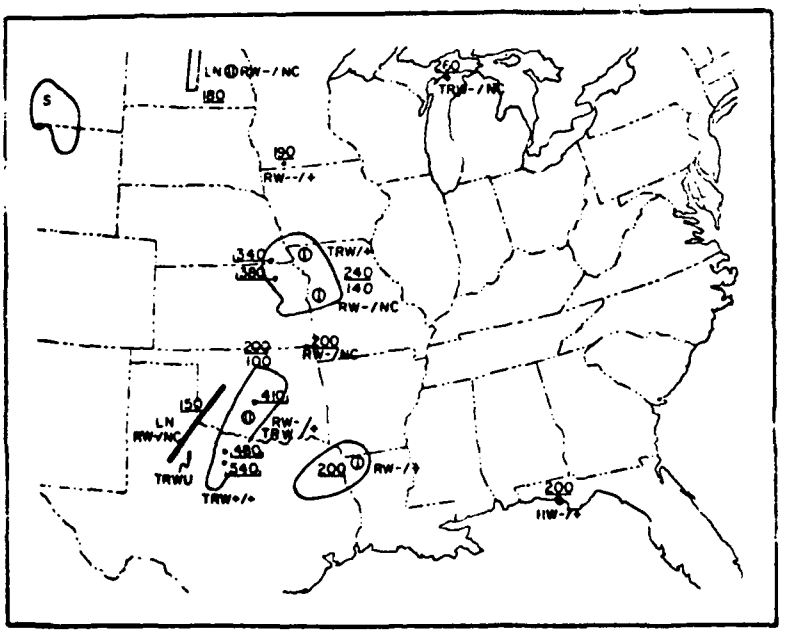

Fig. 16. Radar summary for 1745 GMT 29 April 1970.

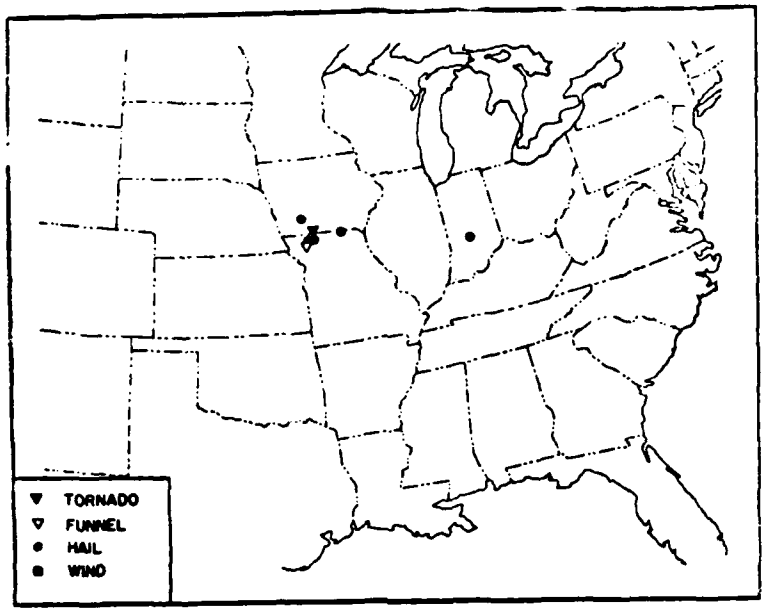

Fig. 17. Severe weather occurrences between 1800 and 2100 GMT 29 April 1970.

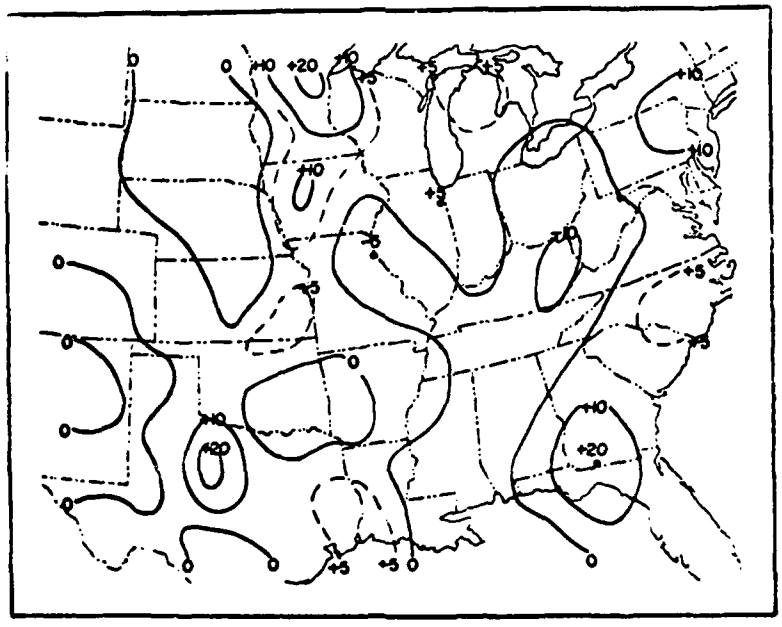

Fig. 18. Horizontal moisture convergence for (x 10 gm kg^{-1} hr^{-1}) 1800 GMT 29 April 1970.

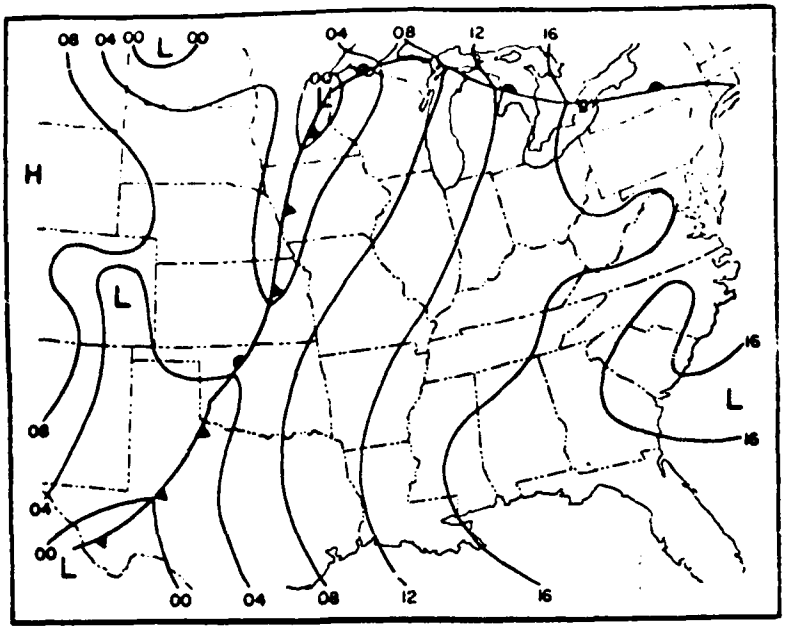

Fig. 19. Surface chart for 2100 GMT 29 April 1970.

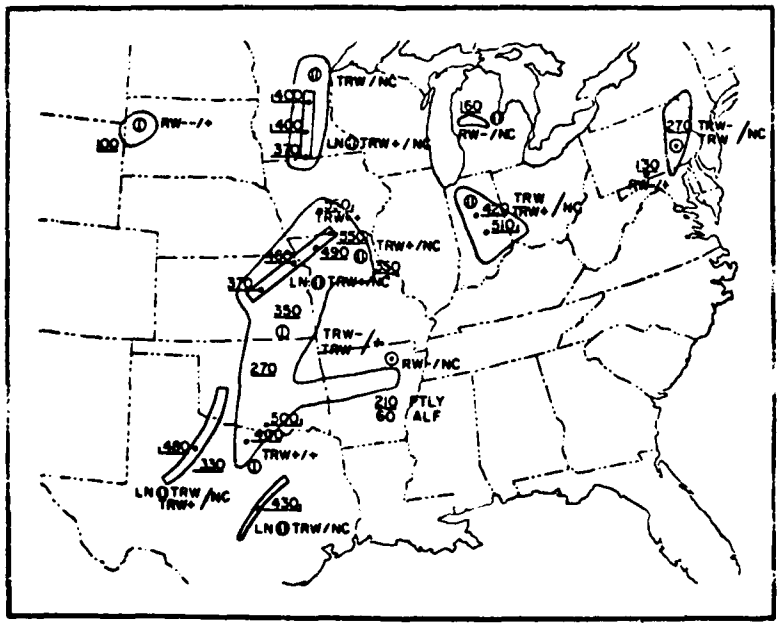

Fig. 20. Radar summary for 2045 GMT 29 April 1970.

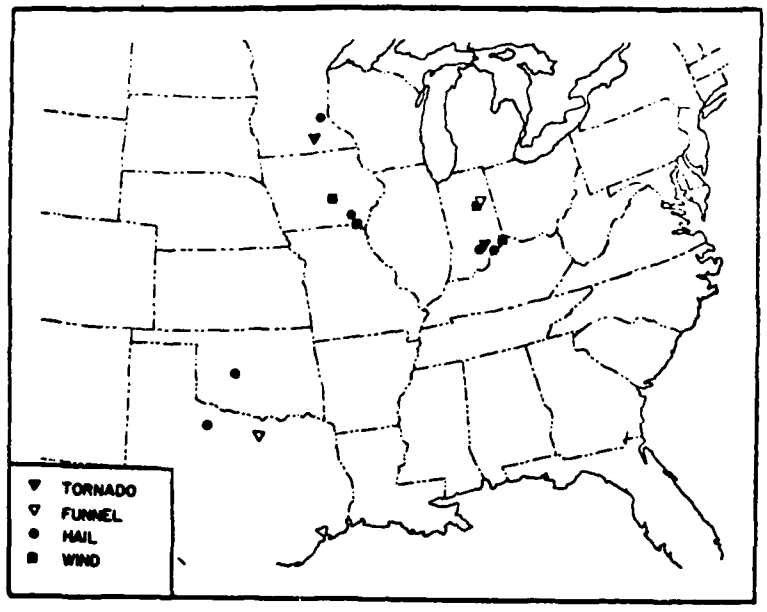

Fig. 21. Severe weather occurrences between 2100 GMT 29 April and 0000 GMT 30 April 1970.

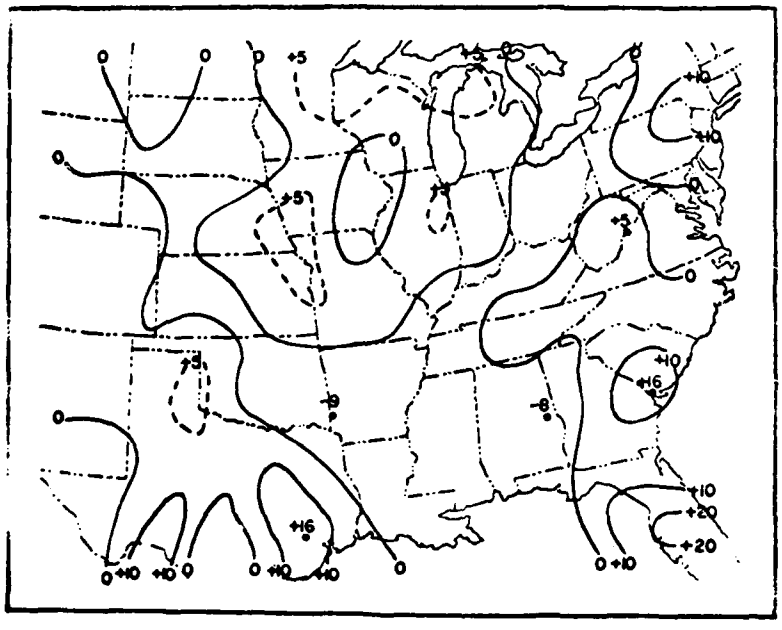

Fig. 22. Horizontal moisture convergence for (x 10 gm kg^{-1} hr^{-1}) 2100 GMT 29 April 1970.

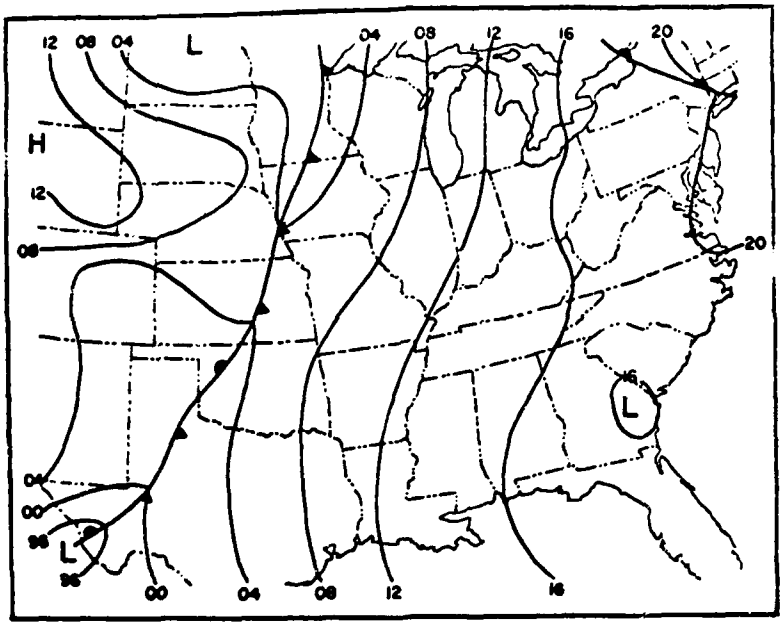

Fig. 23. Surface chart for 0000 GMT 30 April 1970.

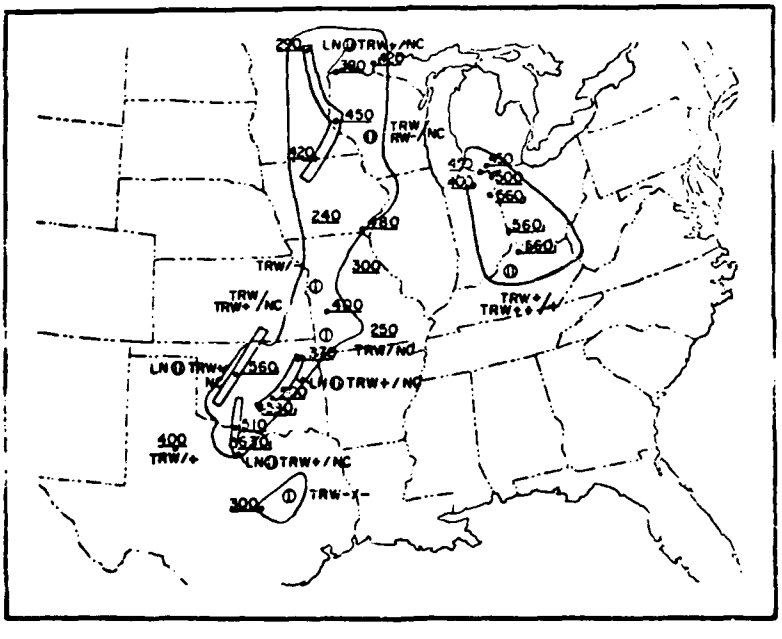

Fig. 24. Radar summary for 2345 GMT 29 April 1970.

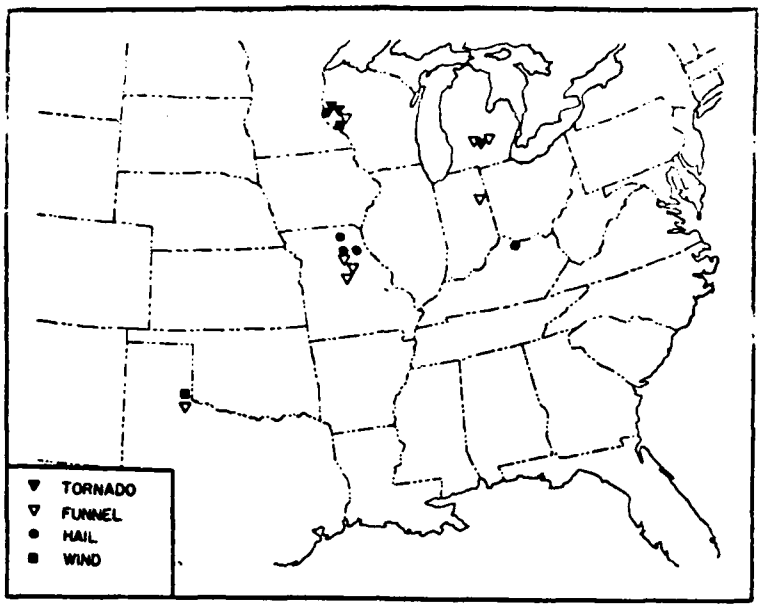

Fig. 25. Severe weather occurrences between 0000 GMT and 0300 GMT 30 April 1970.

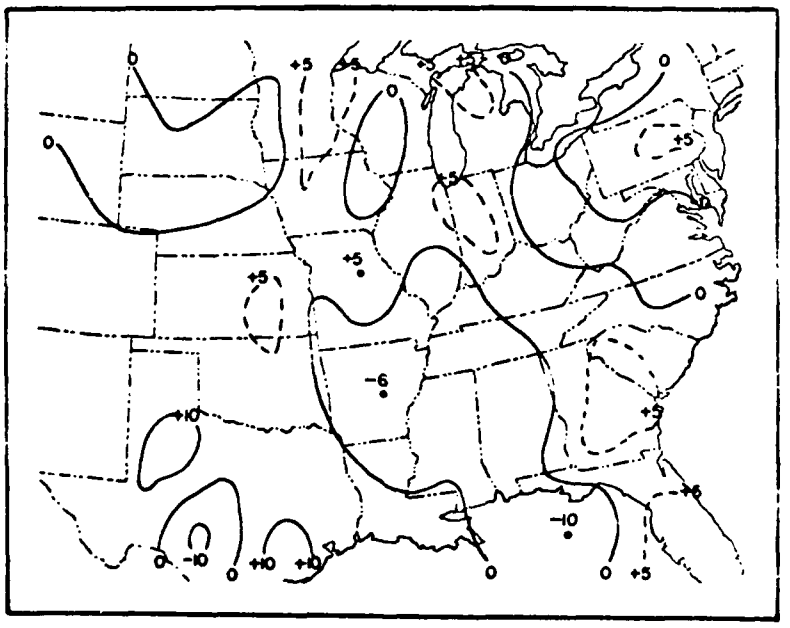

Fig. 26. Horizontal moisture convergence for 0000 GMT 30 April 1970 (x 10 gm kg^{-1} hr^{-1}).

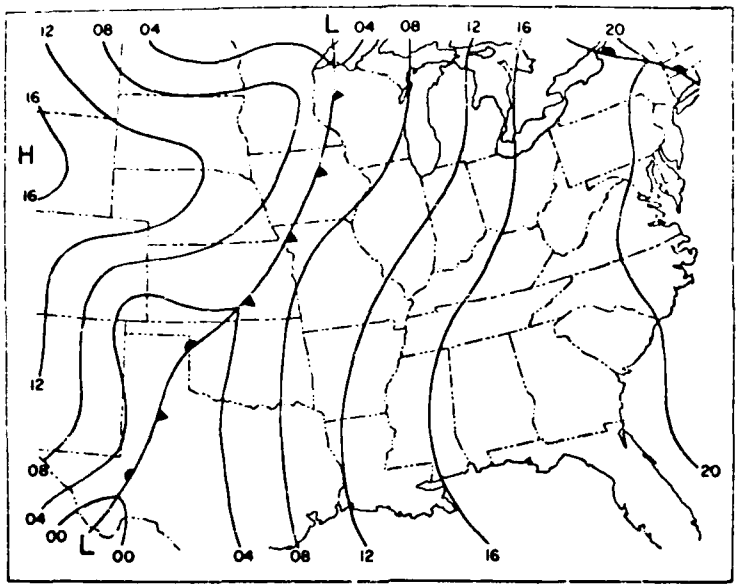

Fig. 27. Surface chart for 0300 GMT 30 April 1970.

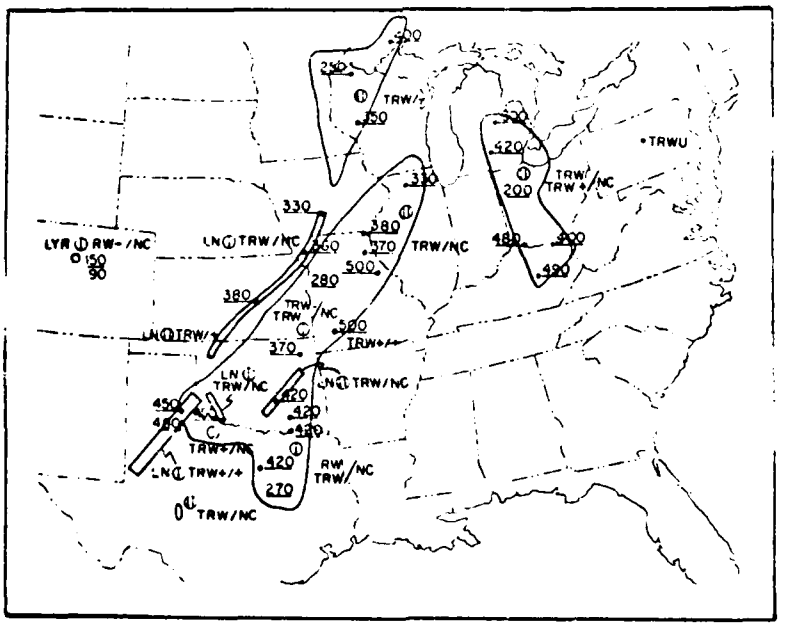

Fig. 28. Radar summary for 0245 GMT 30 April 1970.

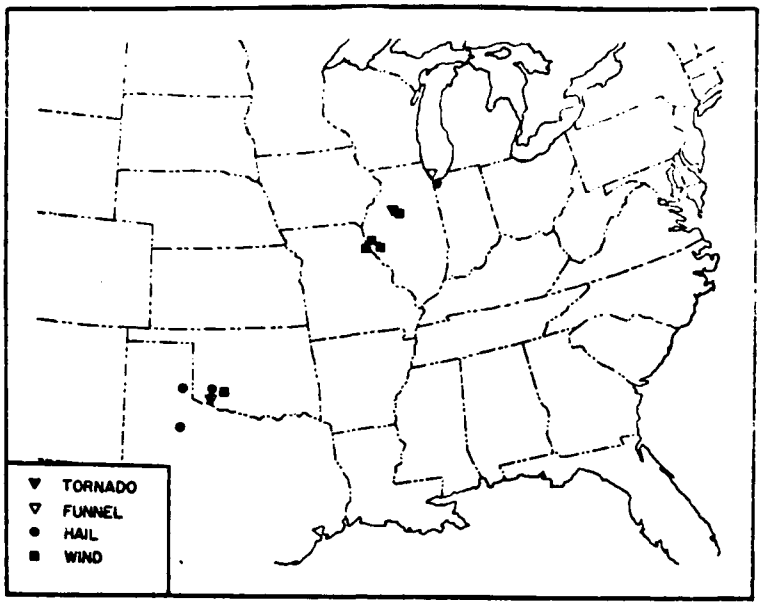

Fig. 29. Severe weather occurrences between 0300 GMT and 0600 GMT 30 April 1970.

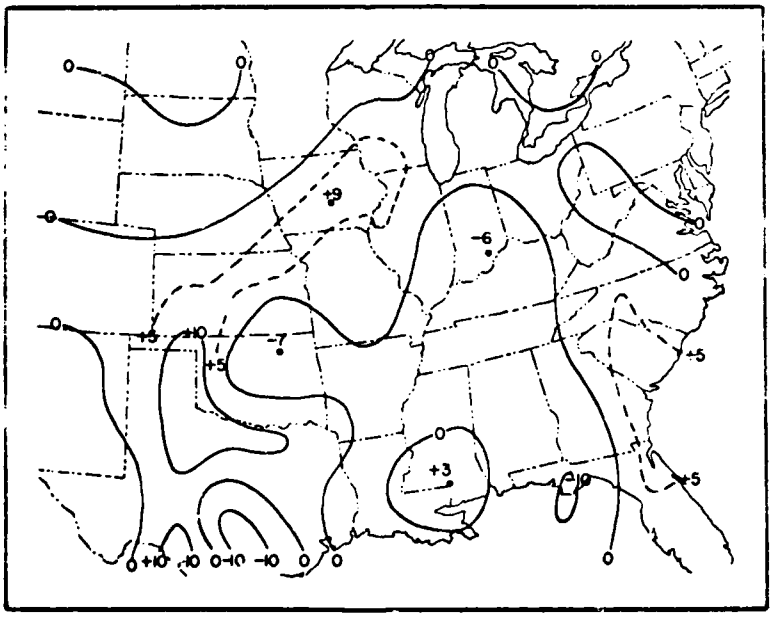

Fig. 30. Horizontal moisture convergence for 0300 GMT 30 April 1970 (x 10 gm kg^{-1} hr^{-1}).

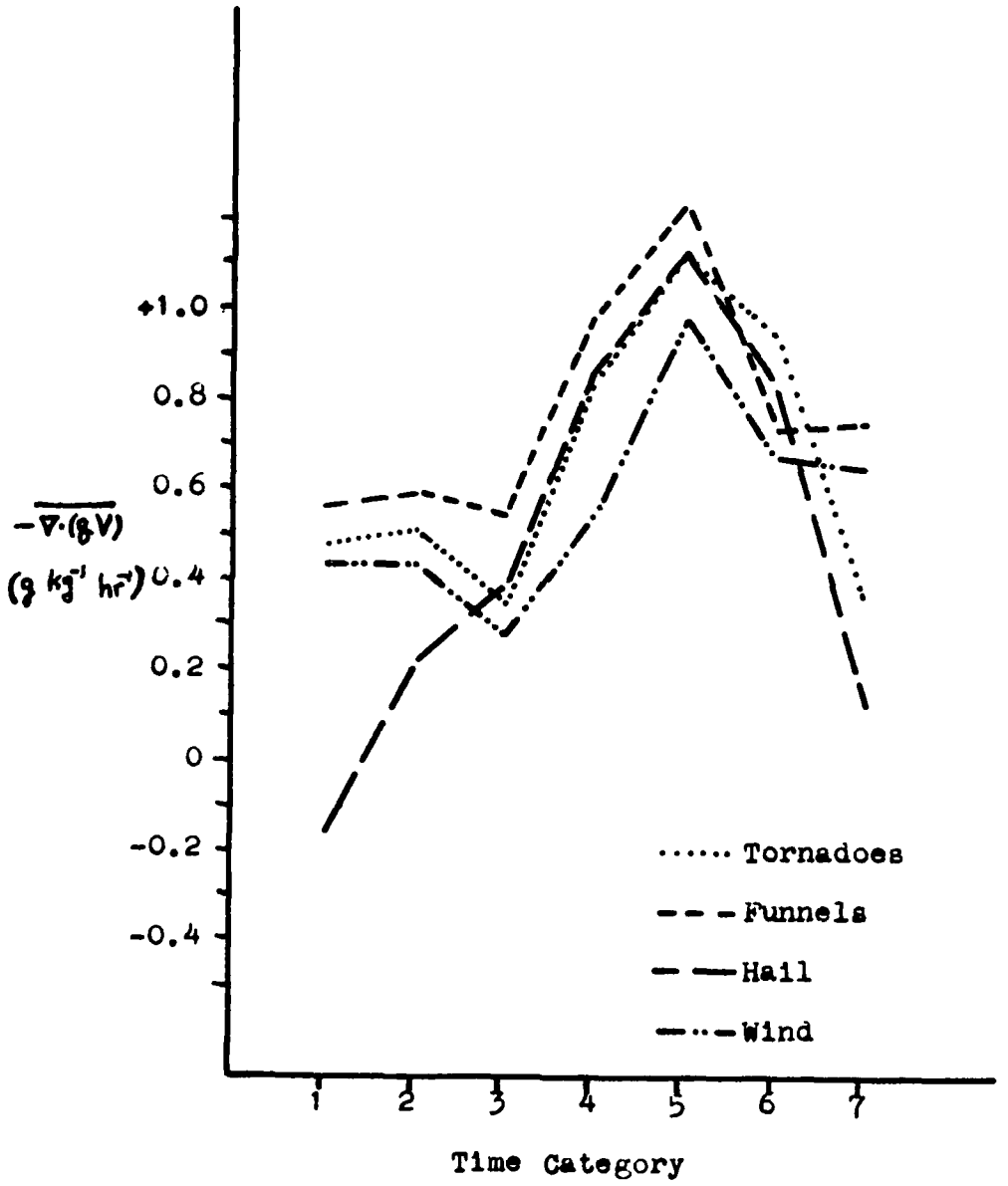

Fig. 31a. Average values of horizontal moisture convergence for 7 time categories for 153 severe weather occurrences during the period 0000 GMT 18 April 1970 to 0000 GMT 20 April 1970.

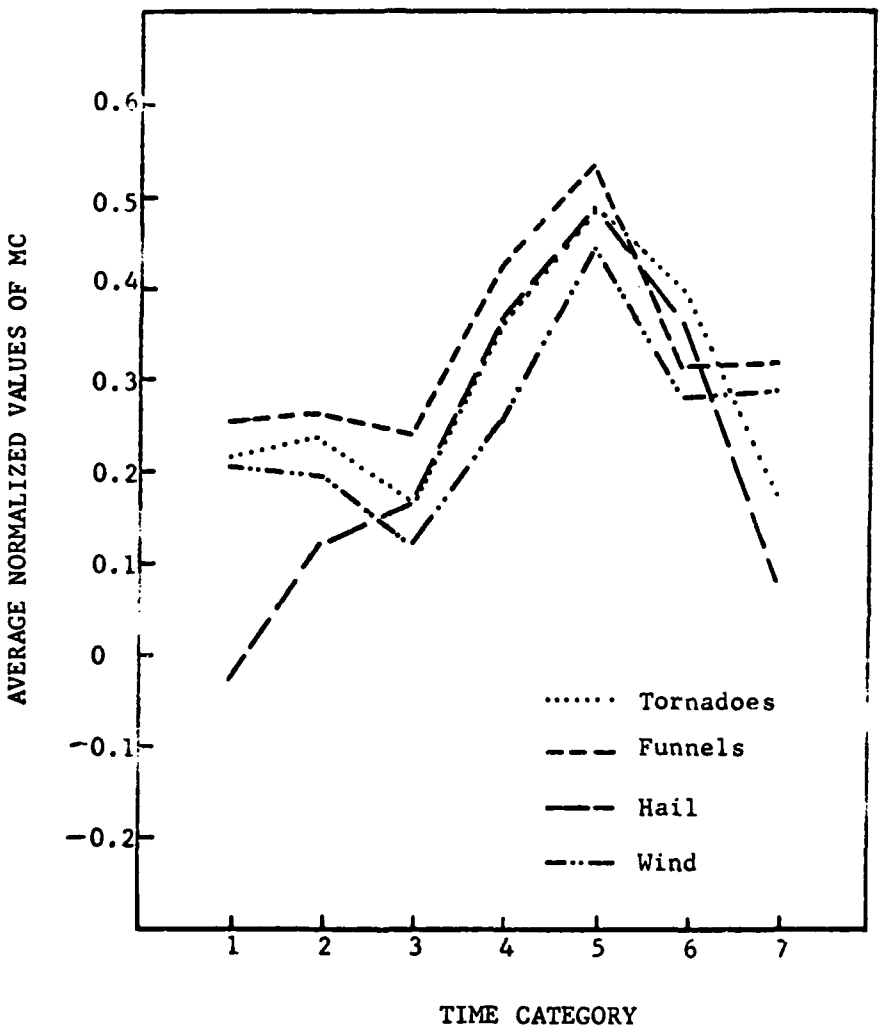

Fig. 31b. Average normalized values of horizontal moisture convergence for 7 time categories for 153 severe weather occurrences during the period 0000 GMT 18 April 1970 to 0000 GMT 20 April 1970.

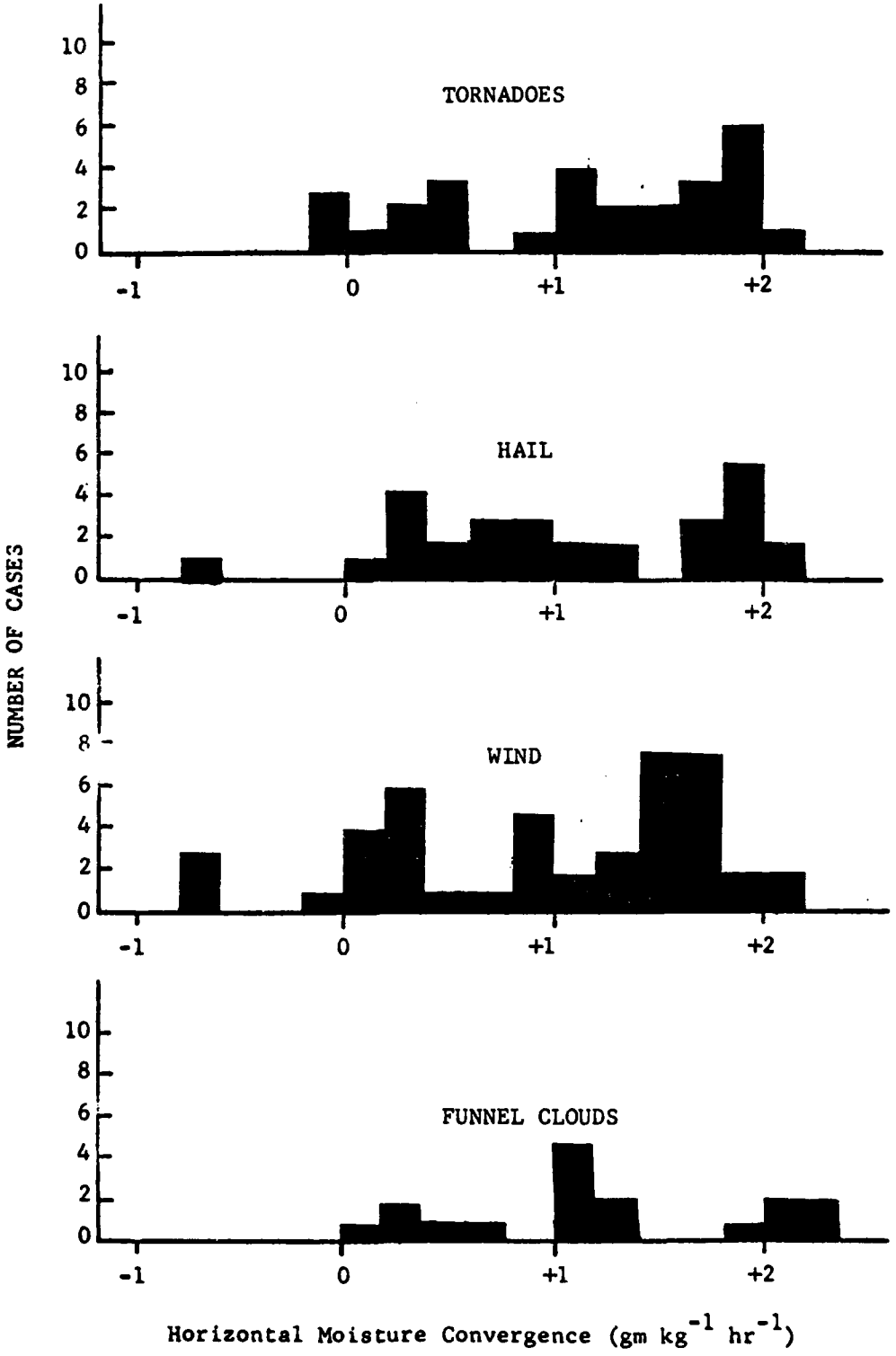

Fig. 32. Range of values of MC for category five.

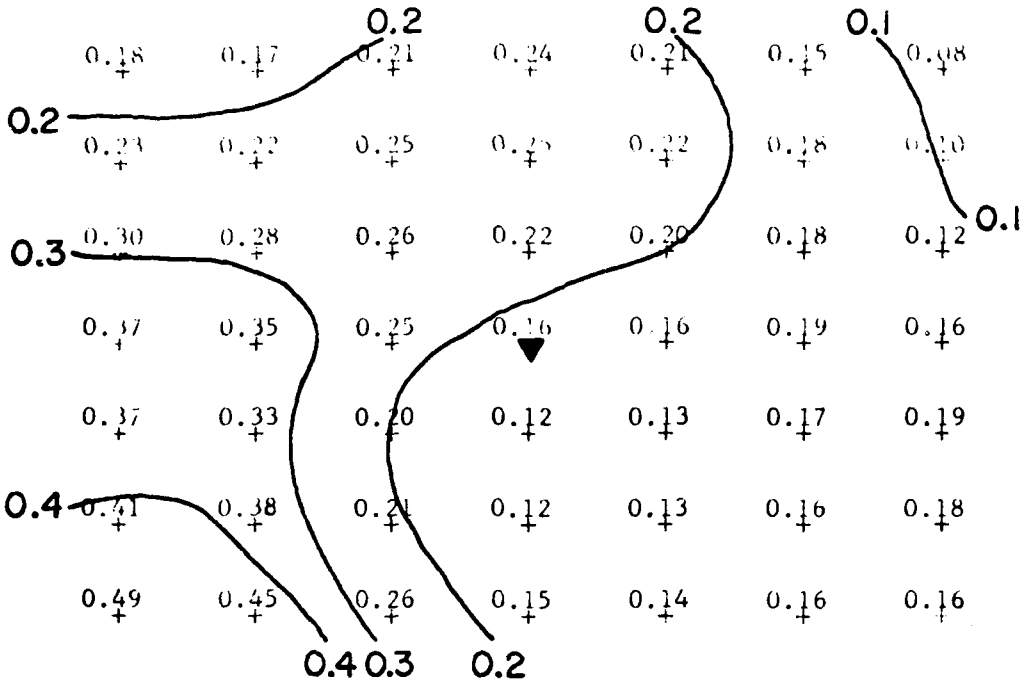

Fig. 33. Normalized pattern of horizontal moisture convergence for 126 severe weather occurrences 6 to 9 hrs before time of occurrence.

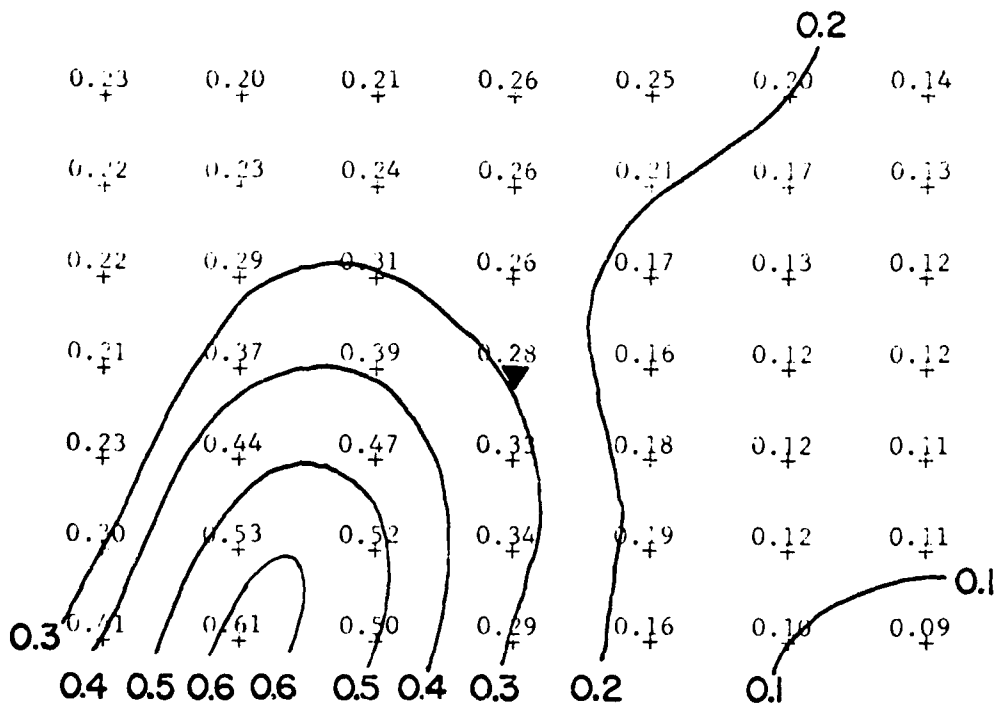

Fig. 34. Normalized pattern of horizontal moisture convergence for 106 severe weather occurrences 3 to 6 hrs before time of occurrence.

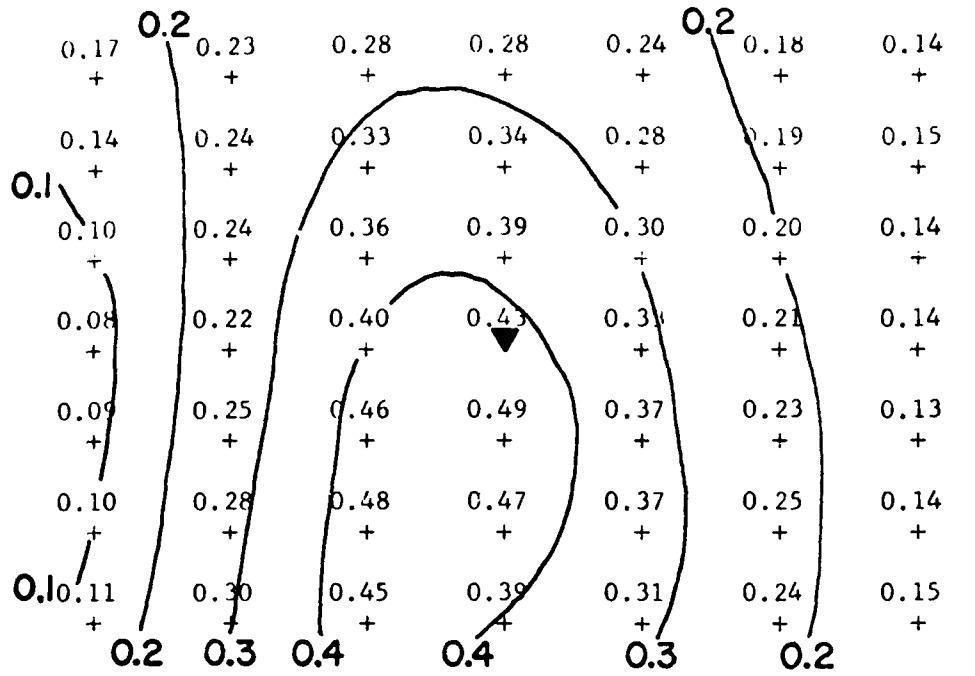

Fig. 35. Normalized pattern of horizontal moisture convergence for 95 severe weather occurrences 0 to 3 hrs before time of occurrence.

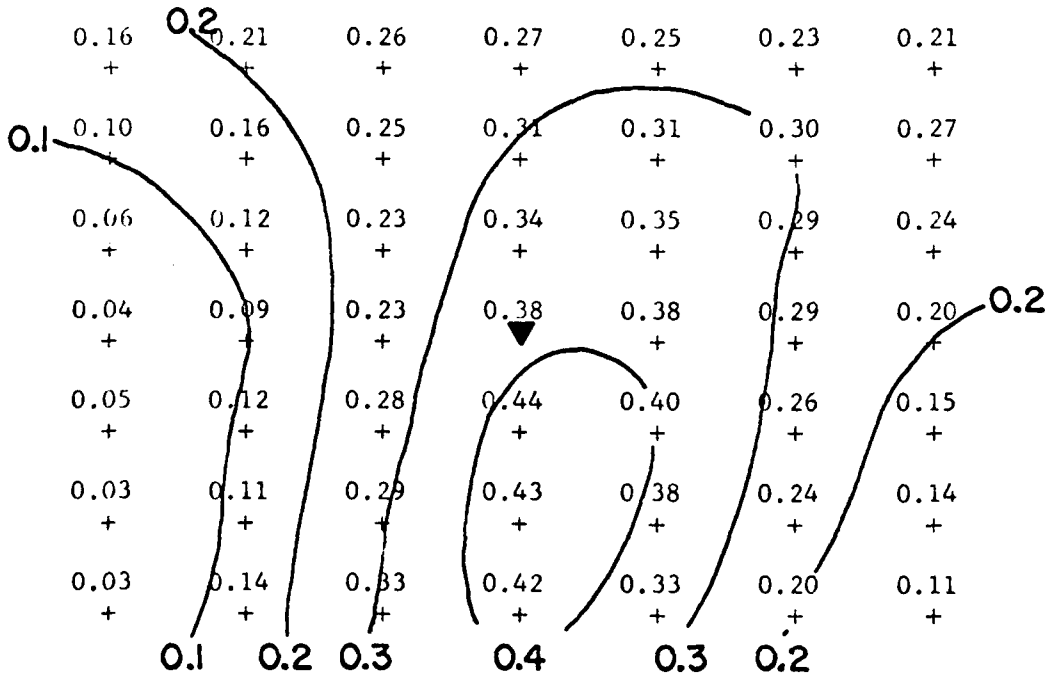

Fig. 36. Normalized pattern of horizontal moisture convergence for 81 severe weather occurrences 0 to 3 hrs after time of occurrence.